

Slowly-modulated two pulse solutions and pulse splitting bifurcations

Arjen Doelman
Korteweg-deVries Instituut
Universiteit van Amsterdam
Plantage Muidergracht 24
1018TV Amsterdam, The Netherlands

Wiktor Eckhaus
Mathematisch Instituut
Universiteit Utrecht
P.O. Box 80.010
3508TA Utrecht, The Netherlands

Tasso J. Kaper
Department of Mathematics
& Center for BioDynamics
Boston University
111 Cummington Street
Boston, MA 02215, U.S.A.

April 23, 1999

Abstract

Two pulse solutions play a central role in the phenomena of self-replicating pulses in 1-D reaction-diffusion systems. In this work, we focus on the 1-D Gray-Scott model as a prototype. We carry out an existence and stability study for solutions consisting of two pulses moving apart from each other with slowly varying velocities. In the various parameter regimes, critical maximum wave speeds are identified, and ODE's are derived for the wave speed and for the separation distance between the pulses. The bifurcations in which these solutions are created and annihilated, and in which they gain stability, are determined. Good agreement is found between these theoretical predictions and the results from numerical simulations. The initial separation distance between the pulses need only be such that the fast (activator) components are exponentially small. In particular, there is no requirement in the analysis on the inhibitor component, which is in fact far away from its homogeneous value, and slowly varying between the pulses, as is critical for the dynamics. Hence, the results presented here apply to the strong pulse interaction problem. Finally, we show how these results may be used to answer central questions about pulse splitting, including how they provide a possible mechanism. The main methods used are analytical and geometric singular perturbation theory for the existence demonstration, and the nonlocal eigenvalue problem (NLEP) method developed in our earlier work for the stability analysis.

1 Introduction

Self-replicating spots and pulses have been observed in excitable reaction-diffusion systems [22, 17, 24, 23, 16, 9, 2, 3, 4, 25, 21, 19, 8]. Spots and pulses are regions in which the concentrations of some of the species exhibit large amplitude perturbations from a surrounding homogeneous state. Depending on system parameters, these regions can enlarge and then subsequently split, so that the spots and pulses replicate themselves in a complex, and as yet incompletely understood, manner.

Two-pulse patterns play a fundamental role in the numerical simulations of pulse-splitting in one-dimensional problems [24, 23, 2, 21]. In order to understand this phenomenon, it is necessary to study the evolution of solutions consisting of pairs of pulses in which the pulses move apart from each other, see Figure 1. The two-pulse solutions studied in this paper move apart with a slowly decreasing velocity. Outside the parameter domain in which the splitting process takes place, the pulses settle down, eventually, in a stationary periodic two-pulse pattern (on a bounded domain). See Figure 2a. In the critical regime where splitting is first observed, the two pulses (or spikes) are observed to move apart from each other with a slowly-decreasing velocity and then to undergo the splitting process when they are nearly stationary. See Figure 2b. Further from critical, the pulses are observed to propagate with constant speed.

In this paper, we carry out an existence and stability analysis for two-pulse patterns in the irreversible one-dimensional Gray-Scott model, [11] (see also the references in [11, 22, 23, 2] for the derivations and early studies of this model):

$$\begin{aligned}\frac{\partial U}{\partial t} &= \frac{\partial^2 U}{\partial x^2} - UV^2 + A(1 - U), \\ \frac{\partial V}{\partial t} &= D \frac{\partial^2 V}{\partial x^2} + UV^2 - BV.\end{aligned}\tag{1.1}$$

For all positive values of the parameters A, B , and D , the background homogeneous state ($U \equiv 1, V \equiv 0$) is stable. The two-pulse solutions considered in this paper are asymptotic to this basic state as $x \rightarrow \pm\infty$. The pulses correspond to excursions of the V -components away from the $V \equiv 0$ background state on narrow intervals; the U -component varies significantly outside these regions and is in general not close to $U \equiv 1$ in between the V -pulses. In particular, we focus on solutions of (1.1) consisting of a pair of pulses, symmetrically disposed about $x = 0$, whose velocities $c(t)$ and $-c(t)$, and as a consequence also their amplitudes, are allowed to vary slowly in time, see Figure 1.

The first main results presented here concern existence of two-pulse solutions when:

$$A/B^2 \ll 1 \quad \text{and} \quad B^3 D/A \leq \mathcal{O}(1).\tag{1.2}$$

Existence is established using methods from analytical and geometric singular perturbation theory. These methods also yield the bifurcations in which these solutions are created. The pulses in these solutions move with slowly-varying wave speeds $c(t)$ that are determined self-consistently by certain ordinary differential equations arising in the analysis. These equations directly give the time courses of $c(t)$, as well as the separation distances $\Gamma(t)$ between the two pulses. We focus especially on determining the allowable intervals of $c(t)$ values, and on identifying the algebraic rates of decay of these $c(t)$. In addition, we show that there is a natural geometric interpretation of the critical (maximum) allowable speeds $c(t)$, and we determine whether or not the minimum values of $c(t)$, namely those values corresponding to fixed points of the equations and hence to traveling or stationary waves, are locally attracting or repelling.

Second, we study the linear stability of the slowly-modulating two-pulse solutions using the NLEP (nonlocal eigenvalue problem) method developed in [3]. The two-pulse solutions undergo subcritical Hopf bifurcations at a certain critical parameter combination, C_{HOPF} at $A = \mathcal{O}(B^2\sqrt{D})$. See Figure 3. For parameter combinations above C_{HOPF} in Figure 3 the solutions are (formally) linearly stable with respect to perturbations that evolve on time scales that are shorter than that of $c = c(t)$. Their instability for parameters just above C_{HOPF} is manifested by large-scale oscillations in the pulse amplitudes.

An overview of the existence and stability results obtained in this paper is given in Figure 3 in the case when D is small. The various curves marking the bifurcations and stability boundaries are shown in the two parameter space with $A = D^\alpha$ and $B = D^\beta$. Of course, we emphasize that Figure 3 represents one regime in which to display the results obtained here, and that they are valid for all parameter combinations that satisfy the principal conditions (1.2), and into the regime $A/B^2 = \mathcal{O}(1)$ (see, however, Remark 1.1). For example, the curve C_{SPLIT} , which corresponds to the scaling $A/B^2 = \mathcal{O}(1)$ in which the splitting occurs, is given by $\beta = \alpha/2$.

Third, we continue the study, that was begun in [3], of the regime $A/B^2 = \mathcal{O}(1)$ in which the self-replication is observed. This regime is represented by the line C_{SPLIT} in Figure 3. In the special scaling used in [3], it was found that there are critical values of the ratio A/B^2 , called $\varepsilon_{\text{split}}$ in this paper, at which the stationary one-pulse solutions (Figure 4) ‘disappear’. This ‘disappearance bifurcation’ was identified as a saddle node bifurcation of homoclinic orbits in the numerical simulations of [21]. The existence of this disappearance or saddle node bifurcation value for $A/B^2 = \varepsilon_{\text{split}}$ was proven by a topological shooting method in Section 6 of [3] for a certain special scaling of A , B and D . In particular, we considered fixed values of A and D and showed that, for each A in the regime considered, there exists a value of B , labeled B_D , at which these solutions disappear. The analysis carries over almost verbatim for the general problem studied here.

The slowly-modulating two-pulse solutions constructed in this paper can be used to describe the evolution and interactions of a pair of pulses created by the splitting of the initial stationary one-pulse pattern. Thus, these solutions can be interpreted as governing the transition between a one-pulse solution that has just split into two and a time asymptotic state in the splitting regime, which is a stable stationary periodic multi-pulse pattern. See Figure 2b and [24, 23, 2, 25, 3, 21, 19].

By extrapolating the insights obtained by the asymptotical analysis into the region $A/B^2 = \mathcal{O}(1)$ we argue (in the final section of this paper) that there is, for the modulating two-pulse solutions, an ‘effective’ scaled value, $\varepsilon = \varepsilon(t)$ of the ratio A/B^2 that varies slowly in time. When the pulses are close together, *i.e.* just after the splitting of the stationary one-pulse pattern (Figure 1a) this effective value is less than the unscaled ratio A/B^2 of the one-pulse. Therefore, the two-pulse pattern can exist when the one-pulse has already ‘disappeared’: the splitting process has effectively reduced A/B^2 below $\varepsilon_{\text{split}}$. However, $\varepsilon(t)$ increases slowly towards the unscaled ratio A/B^2 associated to the one-pulse pattern; and hence, at a certain time, $\varepsilon(t)$ will pass through $\varepsilon_{\text{split}}$ and the two slowly traveling pulses will both split, see Figure 2b. These arguments also predict that the structure of the traveling pulse solutions between successive splittings must be structurally different when A/B^2 is not close to $\varepsilon_{\text{split}}$. This is confirmed by numerical simulations, see Section 8 and [21].

This study of slowly-modulating pulses may be classified as a treatment of a strong pulse interaction problem. Weak pulse interactions take place under the assumption that in between

the two pulses both the U and the V components are close to the background, homogeneous, stable, state (see for instance [8]). A crucial aspect of the analysis in this paper is that the ‘slow’ U component undergoes $\mathcal{O}(1)$ changes away from $U \equiv 1$, see Figure 1. The case of weak pulse interactions can be obtained from the analysis here by taking the limit $t \rightarrow \infty$, so that the pulse are so far apart that $U \approx 1$ in between, see Section 8 and [8].

We study the existence problem by an analytical and a geometric singular perturbation method. In the analytical approach we consider the equations for U and V as (almost) uncoupled problems by assuming that V has a delta-function character in the U -equation and that U is constant in the V -equation (to leading order). The geometric method employed here, which is based on the Fenichel geometric singular perturbation theory [10], is an extension of the method used in [2] to study singular pulse patterns in the Gray-Scott model. There, an invariant slow manifold was identified in the phase space of the system of ordinary differential equations for stationary solutions, and a decomposition of the dynamics was achieved by considering separately the slow dynamics on the invariant manifold and the fast dynamics in the transverse directions. The same type of decomposition of the relevant phase spaces is achieved here. In fact, it is precisely by classifying the dynamics on the slow manifold that one is naturally led to the identification of the various parameter regimes in which the existence of the slowly-modulating two pulse solutions can be established. However, the critical scalings of all relevant quantities are first derived by the analytical singular perturbation method. The relation between these two methods is also discussed.

This paper is organized as follows. Sections 2 and 3 contain the formal perturbation method for stationary and slowly-modulating pulse solutions. Then, in Section 4, the central geometric features of the problem are used to identify the parameter regions in which the distinctly different modulated two pulse solutions will be constructed. Sections 5 and 6 contain the geometric constructions of these solutions. Next, in Section 7, we present the formal linear stability analysis of the different solutions obtained in Sections 3, 5 and 6. The final section (Section 8) provides insight into the central role of the slowly-varying inhibitor concentration $U(x, t)$. It also provides a quantitative comparison between the analytical results and those obtained from numerical simulations, and it concludes with a brief discussion of the ways in which the two methods employed here, namely the analytical and geometric singular perturbation theory, complement each other.

Remark 1.1. The conditions (1.2) are the most important conditions on the parameters A , B and D of (1.1). There is one additional condition, $D \ll 1$ that will appear in the validity analysis of subsection 5.6 and the stability analysis of Section 7. The case $D \geq \mathcal{O}(1)$ turns out to be of little interest since here the pulse solutions cannot be stable, see Remark 7.2. Note, however, that there certainly are stable ‘localized’ patterns for $D = \mathcal{O}(1)$ in a parameter regime that differs from the regime studied here, $AD = \mathcal{O}(B^2)$ ((1.2) implies that $AD \ll B^2$), see [12, 13] for the case $AD = B^2$, $D = 1$.

Remark 1.2. The speeds of moving pulses were also obtained, via numerical simulations, in the papers [24, 25] in which the discovery of self-replicating pulses was reported. There the speeds are given numerically as functions of the differences between the fluxes into the left and right sides of the pulses. They found that certain branches of solutions abruptly appear and/or disappear as the flux difference changes, and that there are transitions from wave speed curves for two-pulse solutions to those for higher-pulse solutions. There are some qualitative similarities between the picture obtained in [24] and that determined analytically here, especially with the presence of the (initial) maximum values of $c(t)$. See also [23].

2 Stationary single pulse solutions

In this section, we present an asymptotic analysis of the stationary single-pulse solutions of the PDE (1.1), see Figure 4. The existence of these solutions was proven in [2] for a special choice of parameters using methods from geometric singular perturbation theory. Our purposes here are to briefly revisit the existence result from a different perspective, to derive the broader scalings for which pulse solutions exist, and to preview the method that will be used in Section 3 on the full problem. The extension of the existence results was briefly announced in Remark 1.1 of [3] (see also [19] for a construction of the stationary spikes).

Stationary solutions of (1.1) are functions $(u(x), v(x))$ for $x \in \mathbf{R}$ satisfying the coupled ODE's

$$\frac{\partial^2 u}{\partial x^2} - uv^2 + A(1 - u) = 0, \quad D \frac{\partial^2 v}{\partial x^2} + uv^2 - Bv = 0. \quad (2.1)$$

A, B and D are independent parameters. Eventually, it will be useful to make special choices about the relative orders of magnitude, but we postpone this as long as possible.

Let $u_0 \equiv [u]_{x=0}$ be the value of u at the center of the pulse (see Figure 1). The v -problem for the pulse is made more transparent by introducing new variables

$$\hat{\xi} = \sqrt{\frac{B}{D}}x \quad \text{and} \quad \hat{v}(\hat{\xi}) = \frac{u_0}{B}v(x). \quad (2.2)$$

Hence,

$$\frac{\partial^2 \hat{v}}{\partial \hat{\xi}^2} + \left(\frac{u(x)}{u_0} \right) \hat{v}^2 - \hat{v} = 0, \quad (2.3)$$

where the quantity u_0 is unknown at this stage. The main goal is to determine the values of u_0 for which stationary single pulse solutions exist.

The basis of the analytic approximation method to be developed in this section is that there is a disparity between the rates of change of u and v . We will see that \hat{v} varies on an $\mathcal{O}(1)$ interval in the $\hat{\xi}$ variable, while significant variation in u only occurs over much longer intervals.

The first step in the analytical method is to derive an approximation for $u(x)$ along a single pulse solution. Treating $v(x)$ in (2.1) as if it was a known function, and putting the term containing v on the right hand side, one gets by a standard procedure:

$$u(x) = 1 - \frac{1}{2\sqrt{A}} \left\{ \int_{-\infty}^x e^{\sqrt{A}(x'-x)} u(x') v^2(x') dx' + \int_x^{\infty} e^{-\sqrt{A}(x'-x)} u(x') v^2(x') dx' \right\}. \quad (2.4)$$

Formula (2.4) constitutes an integral equation for $u(x)$ that may be solved for a given $v(x)$. We note that a pulse-like function $v^2(x)$ should be expected to have a substantial magnitude inside the pulse interval, which is an order $\sqrt{D/B}$ neighborhood of the origin (by virtue of (2.2) and (2.3)), and it should be expected to be virtually zero for x outside this same neighborhood. Also, inside this neighborhood, the functions $u(x')$ and $e^{\pm\sqrt{A}x'}$ are assumed to be slowly varying (see the end of this section for a consistency condition), and it suffices to keep the first (constant) term in their Taylor expansions about $x' (= \hat{\xi}) = 0$ in order to obtain the leading order terms for the integrals in (2.4). Hence, to leading order, the u component of a pulse solution is given by:

$$u(x) = 1 - \frac{u_0}{2\sqrt{A}} \left\{ e^{-\sqrt{A}x} \int_{-\infty}^x v^2(x') dx' + e^{\sqrt{A}x} \int_x^{\infty} v^2(x') dx' \right\}. \quad (2.5)$$

Higher order terms in an asymptotic expansion for $u(x)$ can be constructed by iteration and by using the Taylor expansions of $u(x')$ and the exponential functions in the integrals. The result will be in terms of more and more complicated integrals over $v^2(x)$.

This first approximation (2.5) can be simplified one step further by evaluating the integrals. Since $v(x)$ is insignificant outside of a vanishingly small interval about $x = 0$, the integrals are given to leading order asymptotically by the integrals over the entire real line. Hence, for x outside the small interval in which v^2 is significant, one finds:

$$u(x) \sim 1 - \frac{ku_0}{2\sqrt{A}}e^{\sqrt{A}x}, \quad \text{for } x < 0; \quad u(x) \sim 1 - \frac{ku_0}{2\sqrt{A}}e^{-\sqrt{A}x}, \quad \text{for } x > 0, \quad (2.6)$$

where

$$k = \int_{-\infty}^{\infty} v^2(x')dx'. \quad (2.7)$$

Note that the v -component acts as a delta function in this approximation. Finally, by directly evaluating (2.5) at $x = 0$, one obtains $u_0 = 1 - \frac{ku_0}{2\sqrt{A}}$. Hence, for a given k , the solution is:

$$u_0 = \frac{2\sqrt{A}}{2\sqrt{A} + k}. \quad (2.8)$$

That is, the values of the unknown constant u_0 which correspond to stationary single pulse solutions can be determined as soon as one knows the associated values of the integral k .

In this second step of the analytical method, we derive an approximation for the $v(x)$ component of a single pulse solution that will in turn enable us to determine k . Write (2.3) as:

$$\frac{\partial^2 \hat{v}}{\partial \hat{\xi}^2} + \hat{v}^2 - \hat{v} = \left[\frac{u_0 - u(x)}{u_0} \right] \hat{v}^2. \quad (2.9)$$

The function $u(x)$ varies little near u_0 within the region of the pulse $\hat{\xi} = \mathcal{O}(1)$, so that the right-hand side of (2.9) acts as a perturbation. This suggests approximating $\hat{v}(\hat{\xi})$ by the function

$$\hat{v}_0(\hat{\xi}) = \frac{3}{2} \text{sech}^2 \left(\frac{\hat{\xi}}{2} \right), \quad (2.10)$$

which is the solution of $(\partial^2 \hat{v}_0 / \partial \hat{\xi}^2) + \hat{v}_0^2 - \hat{v}_0 = 0$, with $\hat{v}_0 \rightarrow 0$ as $\hat{\xi} \rightarrow \pm\infty$.

The results from steps one and two above may now be combined to yield approximate solutions for stationary single pulse solutions. Substituting (2.10) into (2.7) and recalling the change of variables in (2.2), one finds after a straightforward calculation:

$$k = 6 \frac{B^{3/2} \sqrt{D}}{u_0^2}. \quad (2.11)$$

Hence, by plugging (2.11) into (2.8), the central unknown u_0 is given by:

$$u_0(1 - u_0) = 3 \frac{B^{3/2} \sqrt{D}}{\sqrt{A}}. \quad (2.12)$$

Therefore, the main goal has now been accomplished, since the solutions of (2.12) give precisely the allowable values of u_0 for stationary one pulse solutions.

Upon examining (2.12) for u_0 , one immediately sees that there are two cases to consider:

$$\text{Case I: } B^{3/2}\sqrt{D/A} \ll 1, \quad \text{Case II: } B^{3/2}\sqrt{D/A} = \mathcal{O}(1) \text{ and } B^{3/2}\sqrt{D/A} < 1/12. \quad (2.13)$$

In Case I, we may Taylor expand both roots of the quadratic (2.12). One solution is:

$$u_0 \sim 3B\sqrt{BD/A}. \quad (2.14)$$

Clearly, in this case, u_0 is asymptotically small, and it is precisely in this case that the existence of one pulse stationary solutions was proven for a special scaling of A, B and D in Theorem 4.1 of [2], see Remark 2.2 below. Moreover, in [3] these solutions were shown to be stable, gaining their stability through a Hopf bifurcation, in a large region of the parameter space.

Remark 2.1. The other root corresponds to an unstable solution of the PDE (1.1). This solution is a ‘weak’ pulse with maximum value for $v(x)$ of $\mathcal{O}(B)$. We expect that this ‘weak’ pulse is unstable, since with $u_0 \sim 1 - 3B\sqrt{BD/A}$, it is a small perturbation of the globally stable homogeneous steady state ($U = 1, V = 0$).

In Case II, both roots of (2.12) are $\mathcal{O}(1)$. The existence of the two associated stationary single-pulse solutions was established in Theorem 4.3 of [2], and both have peaks of height $\mathcal{O}(B)$. Moreover, it was shown (again in the special scaling, though the same analysis can be carried out here) in Theorem 4.3 of [2] that they are born in a saddle-node bifurcation when $B\sqrt{BD/A} = 1/12$.

Having shown how to construct the stationary solutions with $u(x=0) = u_0$ in both cases I and II, we conclude by showing that the perturbation analysis is self-consistent. An important condition emerges that will be imposed globally, except where noted, in the rest of the paper. If one scales the u variable by the size of u_0 (2.14): $u = B^{3/2}\sqrt{D/A}\hat{u}$, and then one substitutes this scaling and those (2.2) of ξ and v into the quasi-stationary ODE for u , one gets:

$$\frac{\partial^2 \hat{u}}{\partial \hat{\xi}^2} = \frac{A}{B^2} \left[\hat{u} \hat{v}^2 - \frac{A}{\sqrt{B}} (1 - B^{3/2} \hat{u}) \right]$$

Hence, in order that the \hat{u} component evolves slowly, we must impose the following global condition:

$$\frac{A}{B^2} \ll 1. \quad (2.15)$$

i.e., the \hat{u} variable evolves slowly in the $\hat{\xi}$ variable relative to the $\mathcal{O}(1)$ rate of change of \hat{v} .

Remark 2.2. In order to compare our results with [2], we set (for this remark only) $D = \delta^2$, where $0 < \delta \ll 1$, $A = \delta^2 a$ and $B = \delta^{2\alpha/3} b$ with $\alpha = 1$ ($\alpha \in [0, 3/2]$ in the analysis in [2], $\alpha = 1$ in most of the numerical simulations in [2]). With these special relations, one solution of (2.12) is $u_0 = (3B^{3/2}/\sqrt{a})\delta[1 + \mathcal{O}(B^{3/2})]$. The corresponding ‘strong’ pulse is then approximated by $v(x) = (1/3)\sqrt{a/B}\delta^{-1/3}\hat{v}_0(\xi)$. For this solution, u_0 is small, and the maximum value of $v(x)$ is large. The results of the asymptotic analysis carried out here for this pulse-solution fully agree with the results of Theorem 4.1 in [2], obtained by geometric methods and the Fenichel theory.

Remark 2.3. The heuristic approximations (2.5) and (2.10) can be made rigorous, under a number of conditions on A, B and D , by converting the full problem (2.9) into an integral equation. Setting $\hat{v} = \hat{v}_0 + \hat{v}_1$, it follows that \hat{v}_1 satisfies the ODE

$$\left(\frac{\partial^2}{\partial \hat{\xi}^2} + 2\hat{v}_0(\hat{\xi}) - 1 \right) \hat{v}_1 = \frac{u_0 - u(x)}{u_0} (\hat{v}_0 + \hat{v}_1)^2 - \hat{v}_1^2 \equiv \mathcal{R}(\hat{v}_0, \hat{v}_1). \quad (2.16)$$

Letting $G(\hat{\xi}, \hat{\xi}')$ denote the Green's function (computed explicitly from the solutions $\psi_1(\hat{\xi}) = (d\hat{v}_0/d\hat{\xi})(\hat{\xi})$ and $\psi_2(\hat{\xi})$ of the homogeneous equation) (2.16) is equivalent to:

$$\hat{v}_1(\hat{\xi}) = \int_{-\infty}^{\infty} G(\hat{\xi}, \hat{\xi}') \mathcal{R}(\hat{v}_0(\hat{\xi}'), \hat{v}_1(\hat{\xi}')) d\hat{\xi}'. \quad (2.17)$$

Higher approximations for $\hat{v}(\hat{\xi})$ can be computed iteratively from this integral equation. Furthermore, viewing (2.4) and (2.17) as a pair of integral equations, one can envision the proof of validity of the first approximations (2.5) and (2.10) by using the contraction mapping principle in a suitably defined Banach space. Such techniques have been used successfully in other nonlinear problems in [7] and [27]; see [27] for a general development of the method. In this manner, one recovers analytically the same results obtained geometrically in Section 4 of [2].

3 Traveling double pulse solutions

In the numerical explorations of [2], it was found that, under various circumstances, one-pulse initial data breaks up into two pulses, one traveling to the right and the other symmetrically to the left. There, the speed of the pulses was found to be of the order asymptotically slow (see Remark 2.1 and Figure 9 in [2]). In this section, we present a method for finding approximations for the traveling double-pulses, especially those for which c is a slowly-varying function of t . In the first subsection, we formulate the framework of a *quasi-stationary approximation* in a moving coordinate system. Next, we construct the solution within that framework and determine the speeds of the pulses. We find that the speed scales as $A\sqrt{D}/B^{3/2}$, which indeed agrees with the numerical simulations in [2] (see Remark 3.2). Furthermore, it varies very slowly with time and tends to zero as $t \rightarrow \infty$.

Remark 3.1. The existence of the pairs of slowly modulated two-pulse solutions is consistent with results from [2], where it was proven that traveling waves that are stationary in a frame moving with constant non-zero speed cannot exist in the parameter regime given studied there (see Remark 2.2): if the two pulses would travel forever (without splitting) then they would each look like a single traveling pulse. Thus, $c(t)$ must approach 0 as $t \rightarrow \infty$.

3.1 The quasi-stationary approximation

Because of the symmetry about $x = 0$, the analysis can be restricted to half of the picture (however, see subsection 5.6). We chose the right-moving pulse on $x > 0$ (see Figure 1). At time t , the center of the pulse is at

$$x = \Gamma(t), \quad \text{where } \Gamma(t) = \int_0^t c(s) ds. \quad (3.1)$$

We also introduce a coordinate attached to the pulse

$$\xi = x - \Gamma(t). \quad (3.2)$$

By (1.1), the equation and boundary conditions for $U(\xi(t), t)$ takes the form:

$$\frac{\partial U}{\partial t} - c \frac{\partial U}{\partial \xi} = \frac{\partial^2 U}{\partial \xi^2} - UV^2 + A(1 - U), \quad (3.3)$$

with the boundary conditions

$$U \rightarrow 1 \quad \text{as} \quad \xi \rightarrow \infty \quad \text{and} \quad \frac{\partial U}{\partial \xi} = 0 \quad \text{for} \quad \xi = -\Gamma(t). \quad (3.4)$$

The second condition in (3.4) arises due to the symmetry of the full problem for $x \in (-\infty, \infty)$: here the right-moving pulse must ‘match’ with the left-moving pulse.

The quasi-stationary approximation consists of imposing the ‘Ansatz’ that $(U(\xi(t), t), V(\xi(t), t))$ only depends on t through $\xi(t)$, *i.e.* $(U(\xi(t), t), V(\xi(t), t)) = (u(\xi(t)), v(\xi(t)))$ where (u, v) does not depend explicitly on t . Thus, the derivative $\frac{\partial U}{\partial t}$ disappears from (3.3): the equation for u is an ODE in which t can be interpreted as a parameter. This parameter appears in $c = c(t)$ and in the position of the boundary condition (3.4). We will see that the construction of singular solutions (in the spirit of the previous section) will imply a relation between $c(t)$ and $\Gamma(t) = \int_0^t c(s) ds$ (for all $t \geq 0$). We refer the reader to subsection 5.6 for an analysis of the consistency and the validity of the quasi-stationary approximation.

In the quasi-stationary approximation, the equation for $v(\xi)$ becomes:

$$-c \frac{\partial v}{\partial \xi} = D \frac{\partial^2 v}{\partial \xi^2} + uv^2 - Bv. \quad (3.5)$$

As in Section 2, this equation becomes more transparent in the new variables (2.2). Recall:

$$\hat{\xi} = \sqrt{\frac{B}{D}} \xi, \quad \hat{v}(\hat{\xi}, t) = \frac{u_0}{B} v(\xi, t), \quad (3.6)$$

where u_0 is again u at $\xi = 0$, but now u_0 depends on the ‘parameter’ time. Hence,

$$\frac{-c}{\sqrt{BD}} \frac{\partial \hat{v}}{\partial \hat{\xi}} = \frac{\partial^2 \hat{v}}{\partial \hat{\xi}^2} + \left(\frac{u}{u_0} \right) \hat{v}^2 - \hat{v}. \quad (3.7)$$

We look for pulse-like solutions for the function $\hat{v}(\hat{\xi}, t)$, that is, solutions that tend rapidly to zero when $|\hat{\xi}|$ is large. Hence, the boundary condition for all t is $\hat{v}(\hat{\xi}, t) \rightarrow 0$ as $|\hat{\xi}| \rightarrow \infty$.

3.2 Approximate solutions for $u(\xi)$

Let

$$\mu_{\pm} \equiv \frac{1}{2} \left(-c \pm \sqrt{c^2 + 4A} \right), \quad (3.8)$$

and note for later reference that when $c^2 \ll A$,

$$\mu_{\pm} \sim \pm \sqrt{A}. \quad (3.9)$$

The general solution of (3.3) in the quasi-stationary limit is now at hand by elementary procedures:

$$u(\xi) = 1 - \frac{1}{(\mu_+ - \mu_-)} \left\{ e^{\mu_- \xi} \int_{-\Gamma(t)}^{\xi} e^{-\mu_- x'} u(x') v^2(x') dx' + e^{\mu_+ \xi} \int_{\xi}^{\infty} e^{-\mu_+ x'} u(x') v^2(x') dx' \right\}$$

$$\left. -\frac{\mu_+}{\mu_-} e^{(\mu_- - \mu_+) \Gamma(t)} e^{\mu_- \xi} \int_{-\Gamma(t)}^{\infty} e^{-\mu_+ x'} u(x') v^2(x') dx' \right\}. \quad (3.10)$$

Matters simplify considerably when one observes, as in Section 2, that the pulse-like function $v(x')$ is expected to be virtually zero outside an order $\sqrt{D/B}$ neighborhood of $x' = 0$. Again, Taylor expanding $u(x')$ and the exponential functions, one obtains:

$$u(\xi) \sim 1 - \frac{u_0}{(\mu_+ - \mu_-)} \left\{ e^{\mu_- \xi} \int_{-\Gamma}^{\xi} v^2(x') dx' + e^{\mu_+ \xi} \int_{\xi}^{\infty} v^2(x') dx' - \frac{\mu_+}{\mu_-} e^{(\mu_- - \mu_+) \Gamma} e^{\mu_- \xi} \int_{-\Gamma}^{\infty} v^2(x') dx' \right\}. \quad (3.11)$$

As noted in Remark 2.3, one can envision a procedure for the construction of higher approximations. Fortunately, the results of Section 5 make this unnecessary.

For values of ξ outside the small interval where $v(\xi)$ is nonzero, further simplification follows:

$$u(\xi) \sim 1 - \frac{k u_0}{(\mu_+ - \mu_-)} \left\{ e^{\mu_- \xi} - \left(\frac{\mu_+}{\mu_-} \right) e^{(\mu_- - \mu_+) \Gamma(t)} e^{\mu_- \xi} \right\} \quad \text{for } \xi > 0, \quad (3.12)$$

$$u(\xi) \sim 1 - \frac{k u_0}{(\mu_+ - \mu_-)} \left\{ e^{\mu_+ \xi} - \left(\frac{\mu_+}{\mu_-} \right) e^{(\mu_- - \mu_+) \Gamma(t)} e^{\mu_- \xi} \right\}, \quad \text{for } \xi < 0, \quad (3.13)$$

where, as before,

$$k = \int_{-\infty}^{\infty} v^2(x') dx'. \quad (3.14)$$

Finally, by evaluating (3.11) at $\xi = 0$, it also follows that to leading order:

$$u_0 = 1 - \frac{k u_0}{(\mu_+ - \mu_-)} \left\{ 1 - \left(\frac{\mu_+}{\mu_-} \right) e^{(\mu_- - \mu_+) \Gamma(t)} \right\}, \quad (3.15)$$

which relates the unknown u_0 and the integral k , which is also unknown at this stage.

3.3 Approximate solutions for $\hat{v}(\hat{\xi})$

Following the same procedure used in Section 2 for the stationary single-pulse solutions, we now develop an approximation for the v component of a slowly-modulated, traveling single pulse. We begin by rewriting the problem (3.7) in the quasi-stationary approximation:

$$\frac{\partial^2 \hat{v}}{\partial \hat{\xi}^2} + \hat{v}^2 - \hat{v} = \left(\frac{u_0 - u}{u_0} \right) \hat{v}^2 - \frac{c}{\sqrt{BD}} \frac{\partial \hat{v}}{\partial \hat{\xi}}, \quad \text{with } \hat{v} \rightarrow 0 \text{ as } |\hat{\xi}| \rightarrow \infty. \quad (3.16)$$

The full equation (3.16) is *not* invariant under the transformation $\hat{\xi} \rightarrow -\hat{\xi}$; and, therefore, the existence of solutions that tend to zero for $\hat{\xi} \rightarrow -\infty$ and $\hat{\xi} \rightarrow +\infty$ is a nontrivial matter. To see this more clearly, we compute an integral of (3.16), as follows. Multiplication by $\partial \hat{v} / \partial \hat{\xi}$ yields:

$$\frac{1}{2} \frac{\partial}{\partial \hat{\xi}} \left(\frac{\partial \hat{v}}{\partial \hat{\xi}} \right)^2 + \frac{1}{3} \frac{u}{u_0} \frac{\partial (\hat{v}^3)}{\partial \hat{\xi}} - \frac{1}{2} \frac{\partial (\hat{v}^2)}{\partial \hat{\xi}} = \frac{-c}{\sqrt{BD}} \left(\frac{\partial \hat{v}}{\partial \hat{\xi}} \right)^2. \quad (3.17)$$

Next, we integrate (3.17) and impose the boundary condition in (3.16) for $\hat{\xi} \rightarrow +\infty$:

$$\frac{1}{2} \left(\frac{\partial \hat{v}}{\partial \hat{\xi}} \right)^2 + \frac{1}{3} \frac{u}{u_0} \hat{v}^3 - \frac{1}{2} \hat{v}^2 = \frac{-c}{\sqrt{BD}} \int_{\hat{\xi}}^{\infty} \left(\frac{\partial \hat{v}}{\partial \hat{\xi}} \right)^2 d\hat{\xi} + \frac{1}{3} \int_{\hat{\xi}}^{\infty} \hat{v}^3 \frac{\partial}{\partial \hat{\xi}} \left(\frac{u}{u_0} \right) d\hat{\xi}. \quad (3.18)$$

Finally, by imposing the boundary condition in (3.16) for $\hat{\xi} \rightarrow -\infty$, one obtains the following nontrivial condition for the existence of a homoclinic orbit:

$$\frac{-c}{\sqrt{BD}} \int_{-\infty}^{\infty} \left(\frac{\partial \hat{v}}{\partial \hat{\xi}} \right)^2 d\hat{\xi} + \frac{1}{3} \int_{-\infty}^{\infty} \hat{v}^3 \frac{\partial}{\partial \hat{\xi}} \left(\frac{u}{u_0} \right) d\hat{\xi} = 0. \quad (3.19)$$

In the analysis here we treat the right hand side of (3.16) as a perturbation and approximate the function \hat{v} by the unperturbed solution (2.10). The first term can be expected to be small, because $u(x)$ varies little in the pulse interval, which is of $\mathcal{O}(1)$ width in $\hat{\xi}$. The second term is small if $\frac{c}{\sqrt{BD}} \ll 1$. The pulse velocity c is, of course, unknown yet; naturally, in the final results, c will depend on A, B , and D . Our strategy will be to determine c under the assumption that the right hand side of (3.16) is a perturbation and then verify *a posteriori* (subsection 3.5) under what conditions on the parameters the perturbation assumption is satisfied.

3.4 Computation and analysis of the pulse velocity

In order to carry out a leading order asymptotic analysis of the condition (3.19), $\hat{v}(\hat{\xi})$ may be replaced by the presumed first approximation $\hat{v}_0(\hat{\xi})$ given in (2.10). Also, for a single stationary pulse solution centered at $\hat{\xi} = 0$, it may be readily shown, via a calculation in the original ξ variable, that the term involving the derivative of u has the following form:

$$\frac{\partial}{\partial \hat{\xi}} \left(\frac{u}{u_0} \right) = \left[\frac{\partial}{\partial \hat{\xi}} \left(\frac{u}{u_0} \right) \right]_{\hat{\xi}=0} + \tilde{f}(\hat{\xi}) + \text{h.o.t.}, \quad (3.20)$$

where $\tilde{f}(\hat{\xi})$ is an odd function of $\hat{\xi}$. In particular, for $\xi = \mathcal{O}(\sqrt{D/B})$, the by-now standard approximations imply that equation (3.10) yields to leading order:

$$\frac{\partial u}{\partial \xi}(\xi) = \frac{-u_0}{(\mu_+ - \mu_-)} \left\{ \mu_- \int_{-\Gamma(t)}^{\xi} v^2 dx' + \mu_+ \int_{\xi}^{\infty} v^2 dx' - \mu_+ e^{-(\mu_+ - \mu_-)\Gamma} \int_{-\Gamma}^{\infty} v^2 dx' \right\}. \quad (3.21)$$

The higher order terms introduce a relative error of $\mathcal{O}(\sqrt{AD/B})$. Then, $\int_{-\Gamma}^0 v^2 \sim \int_{-\infty}^0 v^2$ and $\int_{-\Gamma}^{\xi} v^2 \sim \int_{-\infty}^{\xi} v^2$, since the tails $\int_{-\infty}^{-\Gamma} v^2$ are exponentially small. Also, the function $\hat{v}_0(\hat{\xi})$ is symmetric about $\hat{\xi} = 0$, so that $\int_{-\infty}^0 v^2 dx' = \int_0^{\infty} v^2 dx'$ to leading order. Hence, (3.21) reduces to:

$$\frac{\partial u}{\partial \xi}(\xi) = \frac{ku_0}{(\mu_+ - \mu_-)} \left[\frac{c}{2} + \mu_+ e^{-(\mu_+ - \mu_-)\Gamma(t)} \right] + u_0 \tilde{f}(\xi), \quad (3.22)$$

where $\tilde{f}(\xi) \equiv \frac{1}{2} \int_{-\infty}^{\xi} v^2(x') dx' - \frac{1}{2} \int_{\xi}^{\infty} v^2(x') dx'$ and where k is defined in (3.14). Clearly, $\tilde{f}(\xi)$ is antisymmetric about $\xi = 0$. Finally, using (2.11) to evaluate k , recalling the definitions (3.8) of μ_{\pm} , converting to $\hat{\xi}$, and dividing both sides by u_0 , we get to leading order:

$$\left(\frac{\partial}{\partial \hat{\xi}} \frac{u}{u_0} \right) (\hat{\xi}) = 3 \frac{BD}{u_0^2} \left\{ e^{-\sqrt{c^2+4A}\Gamma(t)} + \frac{c}{\sqrt{c^2+4A}} [1 - e^{-\sqrt{c^2+4A}\Gamma(t)}] \right\} + \tilde{f}(\hat{\xi}). \quad (3.23)$$

Hence, we arrive at (3.20): the first term on the right hand side of (3.23) is $(\partial/\partial\hat{\xi})(u/u_0)$ at $\hat{\xi} = 0$, and the second term is antisymmetric about $\hat{\xi} = 0$, as claimed above.

Since \tilde{f} is odd, the integral of $\hat{v}^3 \tilde{f}$ in (3.19) vanishes to leading order, and the condition for the existence of one pulse solutions simplifies to:

$$\frac{-c}{\sqrt{BD}} \int_{-\infty}^{\infty} \left(\frac{\partial \hat{v}_0}{\partial \hat{\xi}} \right)^2 d\hat{\xi} + \frac{1}{3} \left[\frac{\partial}{\partial \hat{\xi}} \left(\frac{u}{u_0} \right) \right]_{\hat{\xi}=0} \int_{-\infty}^{\infty} \hat{v}_0^3(\hat{\xi}) d\hat{\xi} = 0. \quad (3.24)$$

Evaluating the integrals using (2.10), one obtains:

$$\frac{-c}{\sqrt{BD}} + 2 \left[\frac{\partial}{\partial \hat{\xi}} \left(\frac{u}{u_0} \right) \right]_{\hat{\xi}=0} = 0. \quad (3.25)$$

Next, the values of u_0 can be explicitly determined. Using (3.15) and (2.11), we find:

$$u_0(1 - u_0) = 6 \frac{B^{3/2} \sqrt{D}}{(\mu_+ - \mu_-)} \left[1 - \left(\frac{\mu_+}{\mu_-} \right) e^{-(\mu_+ - \mu_-)\Gamma} \right]. \quad (3.26)$$

Now, just as in the analysis of (2.12) in Section 2, there are two cases to consider:

$$\text{Case I: } B^{3/2} \sqrt{\frac{D}{A}} \ll 1 \quad \text{and} \quad \text{Case II: } B^{3/2} \sqrt{\frac{D}{A}} = \mathcal{O}(1). \quad (3.27)$$

Moreover, in both cases, one needs to consider two possibilities: $c^2 \ll A$ and $c^2/A = \mathcal{O}(1)$. We will refer to these as subcases **a** and **b**, respectively. We analyze Case **Ia** in this subsection (and geometrically in Section 5), and in Section 6, we will analyze Cases **Ib** and **IIa** geometrically (see Remark 6.1 for an approach along the lines of this section).

In Case **I**, the quadratic (3.26) has two real solutions, and we are interested in the smaller one:

$$(u_0)_- \sim \frac{6B^{3/2} \sqrt{D}}{(\mu_+ - \mu_-)} \left\{ 1 - \left(\frac{\mu_+}{\mu_-} \right) e^{-(\mu_+ - \mu_-)\Gamma} \right\}. \quad (3.28)$$

This solution clearly reduces to (2.14) obtained in Section 2 for the case of a stationary single pulse (take $t \rightarrow \infty$ where $c = 0$). Moreover, it indicates that the method employed here, which is based on the separation of scales, is consistent if we impose the global condition $A \ll B^2$ given in (2.15). For completeness, we note that, just as we saw in Section 2, the second solution has a value of u_0 that is just below one. The corresponding solution is, therefore, only a small perturbation of the globally stable homogeneous state ($U = 1, V = 0$), and hence it is expected to be unstable.

Specializing to Case **Ia**, we see by (3.8) that (3.23) and (3.28) simplify (to leading order) to:

$$\left[\frac{\partial}{\partial \hat{\xi}} \left(\frac{u}{u_0} \right) \right]_{\hat{\xi}=0} = \frac{3BD}{u_0^2} e^{-2\sqrt{A}\Gamma(t)}, \quad \text{and} \quad (u_0)_- \sim 3\sqrt{\frac{D}{A}} B^{3/2} \left\{ 1 + e^{-2\sqrt{A}\Gamma(t)} \right\}. \quad (3.29)$$

Hence, by using (3.29) in (3.25), we get to leading order:

$$c = \frac{2A\sqrt{D}}{3B^{3/2}} \frac{e^{-2\sqrt{A}\Gamma(t)}}{\left[1 + e^{-2\sqrt{A}\Gamma(t)} \right]^2}, \quad (3.30)$$

where we recall (3.1) that $\Gamma(t)$ is defined as $\Gamma(t) = \int_0^t c(s) ds$. Since $B^{3/2} \sqrt{D/A} \ll 1$ (Case I) and $A \ll B^2$ (by (2.15)), we find $c(t) \ll 1$ for (3.30). Thus, this formula for $c(t)$ corresponds to a slowly propagating pulse solution whose wave speed decreases slowly in time.

Finally, recalling (3.1), we see that (3.30) can also be viewed as a differential equation:

$$\frac{d\Gamma}{dt} = \frac{2}{3} \frac{A\sqrt{D}}{B^{3/2}} \frac{e^{-2\sqrt{A}\Gamma}}{[1 + e^{-2\sqrt{A}\Gamma}]^2}. \quad (3.31)$$

There are no critical points for finite Γ in (3.31), and hence Γ grows without bound.

The equation (3.31) can be solved in an implicit form, but not much insight is gained. Instead, we finish with an ODE for $c(t)$ that can be obtained by differentiating (3.30) by t and by a little algebra (in particular, view (3.30) as a quadratic in $e^{-2\sqrt{A}\Gamma}$ and solve it, taking the root with the minus sign; then, plug this root into the right hand side of the formula for dc/dt), we find:

$$\frac{dc}{dt} = -2\sqrt{A}c^2 \sqrt{1 - \frac{6cB^{3/2}}{A\sqrt{D}}}. \quad (3.32)$$

Hence, $c(t)$ decreases algebraically until the wave is asymptotically stationary. In addition, there is an upper bound for $c(t)$, whose origin we will see from the geometric approach in Section 5.

Remark 3.2. In the numerical simulations for [2] $D = \delta^2$, $A = \mathcal{O}(\delta^2)$, $B = \mathcal{O}(\delta^{2\alpha/3})$, and typically $\alpha = 1$. Hence, (3.30) satisfies: $c(t) = \mathcal{O}(A\sqrt{D}/B^{3/2}) = \mathcal{O}(\delta^2)$, as observed in Figure 9 of [2].

3.5 Consistency of the approximations and a mechanism for the pulse-splitting bifurcation

In this subsection, we analyze the conditions under which the right hand side of (3.16) is indeed a perturbation. There are two terms to consider. By (3.30), it follows that $c/\sqrt{BD} = (A/B^2)\hat{c}$, where $\hat{c} = \mathcal{O}(1)$, and hence the second term on the right hand side of (3.16) is a perturbation if the global condition (2.15) holds.

To analyze the first term, we expand $u(\hat{\xi})$ in a Taylor series:

$$\frac{u_0 - u}{u_0} = - \left[\frac{\partial}{\partial \hat{\xi}} \left(\frac{u}{u_0} \right) \right]_{\hat{\xi}=0} \hat{\xi} - \frac{1}{2} \left[\frac{\partial^2}{\partial \hat{\xi}^2} \left(\frac{u}{u_0} \right) \right]_{\hat{\xi}=0} \hat{\xi}^2 - \dots \quad (3.33)$$

The coefficient of the first term in (3.33) is given by (3.29). Next, the coefficient of the second term is readily computed to leading order from the quasi-static limit of the differential equation (3.3):

$$\left[\frac{\partial^2}{\partial \hat{\xi}^2} \left(\frac{u}{u_0} \right) \right]_{\hat{\xi}=0} = \frac{A}{4B^2} \frac{1}{[1 + e^{-2\sqrt{A}\Gamma}]^2}. \quad (3.34)$$

This leading order term comes directly from the uv^2 term in (3.3), and we note that the A term in (3.3) is higher order, because $\sqrt{AD/B} \ll 1$ in Case I by (2.15). Hence, condition (2.15) also assures the smallness of the first term on the right hand side of (3.16).

To conclude this section, we venture an explanation for the numerically-observed phenomenon that, in a suitably chosen regime of the parameter space, a traveling pulse, *after some time*, splits into a right and left traveling pulse. Consider B as a bifurcation parameter by setting $B^2 = \mathcal{O}(A^{1-\nu})$ with $\nu > 0$. The right hand side of (3.16) ceases to be a perturbation as $\nu \rightarrow 0$, and our construction breaks down. So, let us suppose now that we take ν positive but small, yet such that all coefficients on the right hand side of (3.16) are still numerically sufficiently small for the perturbation assumption to be valid. Then, as time goes on, the coefficient on the first term in the Taylor expansion becomes even smaller because $\hat{c} \rightarrow 0$ (3.30); however, the coefficient (3.34) of the second term in the Taylor expansion grows as $t \rightarrow \infty$, and in fact can grow up to four times its initial value. Moreover, the leading order coefficients on all terms of fourth-, sixth-, ... order in the Taylor expansion will also grow. Therefore, it can happen that, after some time, the perturbation assumption is no longer valid. See also Section 8 for a more detailed discussion.

The time needed for the pulse to break up is smaller if ν is smaller, and hence B is closer to \sqrt{A} , which is precisely the threshold case discovered in [3] and observed there to agree with the splitting bifurcations in numerical simulations. The time-scale relevant to break up can be estimated by the equation for $\Gamma(t)$ (3.31): the time-dependent factor in (3.34) decreases from being near 1 to being $\ll 1$ when $\sqrt{A}\Gamma \gg 1$ on a time scale $\tau = (A\sqrt{AD}/B\sqrt{B})t$ (see also section 5.6). However, $\Gamma(t)$ only grows logarithmically slow on this time scale (by (3.31)). Therefore, the actual splitting will occur after a very long, but $\mathcal{O}(1)$, time T_{split} on this τ time scale. For instance, with A , B and D as in the simulations of Figure 2b we find that $t \approx 175\tau$ so that $T_{\text{split}} \approx 40\tau$. This agrees qualitatively with the dynamics of (3.31).

4 Geometry of governing equations

In this section, we identify the central geometric structures in the equations for modulating two-pulse solutions. This geometric information is essential to proving the existence of these solutions using the Fenichel singular perturbation theory, and it also provides a clear framework to determine the dynamics in each of the parameter regimes, teasing apart the geometric features of Cases **Ia-IIb**. Before describing this geometry, we briefly review essential facts about the modulating two-pulse solutions constructed in Section 3, especially to collect the associated scalings.

In the quasi-stationary approximation, $U(x, t) = u(\xi(t))$ and $V(x, t) = v(\xi(t))$, and the Gray-Scott model (1.1) is:

$$u_{\xi\xi} + c(t)u_{\xi} - uv^2 + A(1 - u) = 0, \quad Dv_{\xi\xi} + c(t)v_{\xi} + uv^2 - Bv = 0. \quad (4.1)$$

where $\xi \equiv x - \int_0^t c(s)ds$ (3.2). At each instant of time t , a modulating two-pulse solution consists of a right moving pulse ($c(t)$) and a left moving pulse ($-c(t)$), symmetric about $x = 0$ (Figure 1). The right-moving pulse solution consists of three segments: a narrow interval in which the v component exhibits a high peak (and u a minimum) centered at $\xi = 0$, *i.e.*, $x = +\int_0^t c(s)ds$ and intervals on either side of the peak in which the v component is exponentially small (and u changes slowly). The v peak corresponds to a fast excursion near the homoclinic orbit of the fast reduced system associated to (4.1). The tails on either side of the pulse are matched to the slow solutions on the left and right intervals. Finally, the left slow solution satisfies Neumann conditions at $x = 0$, and the right slow solution satisfies $u \rightarrow 1$ and $v \rightarrow 0$ as $\xi \rightarrow \infty$.

4.1 Scalings

The analysis of Section 3, in particular (3.6), (3.29), and (3.30), suggests the scalings:

$$\xi = \sqrt{\frac{D}{B}}\hat{\xi}, \quad u(\xi) = B^{3/2}\sqrt{\frac{D}{A}}\hat{u}(\hat{\xi}), \quad v(\xi) = \sqrt{\frac{A}{BD}}\hat{v}(\hat{\xi}), \quad c(t) \equiv \frac{A\sqrt{D}}{B^{3/2}}\hat{c}(t), \quad (4.2)$$

The scaling of ξ corresponds to a stretching of the narrow interval to which the pulse is confined at any given moment in time. To leading order (4.1) becomes:

$$\begin{aligned} \hat{u}_{\hat{\xi}\hat{\xi}} &= \frac{A}{B^2} \left[\hat{u}\hat{v}^2 - D\hat{c}(t)\hat{u}_{\hat{\xi}} + \frac{\sqrt{A}\sqrt{D}}{\sqrt{B}} \left(1 - \frac{B\sqrt{B}\sqrt{D}}{\sqrt{A}}\hat{u} \right) \right], \\ \hat{v}_{\hat{\xi}\hat{\xi}} + \frac{A}{B^2}\hat{c}(t)\hat{v}_{\hat{\xi}} + \hat{u}\hat{v}^2 - \hat{v} &= 0. \end{aligned} \quad (4.3)$$

Again, one clearly sees the origin of the global condition (2.15), namely $A \ll B^2$, which was made so that \hat{u} evolves on a longer space scale than \hat{v} . We remark that the boundary scaling $A/B^2 = \mathcal{O}(1)$, which is intimately connected to the observed pulse splitting, is analyzed in [3], where it is shown that the solutions disappear for a critical value of B , called B_d there. Further results for this scaling are given here in subsection 3.5 and in Section 8.

Next, during the course of the analysis in Sections 2 and 3, we determined (see (2.13), (3.27)) that it was useful to distinguish between two cases:

$$\text{Case I: } B^{3/2}\sqrt{D/A} \ll 1, \quad \text{and} \quad \text{Case II: } B^{3/2}\sqrt{D/A} = \mathcal{O}(1). \quad (4.4)$$

In addition, within each of these two main cases, it was necessary to distinguish between subcases **a** and **b**: $c^2 \ll A$ and $c^2 = \mathcal{O}(A)$, respectively, *i.e.* by (4.2) $AD \ll B^3$ and $AD = \mathcal{O}(B^3)$ respectively. As we shall see in subsection 4.2, the geometry of the slow (outer) subsystem is fundamentally different in each of the four cases **Ia-IIb**.

Finally, the global condition (2.15) and the scalings (4.2) suggest introducing:

$$\varepsilon = \frac{\sqrt{A}}{B} \quad \text{and} \quad \delta = \sqrt{BD}. \quad (4.5)$$

One directly observes that $\varepsilon \ll 1$ due to (2.15), and $\delta \ll 1$ due to both (2.15) and (4.4). Also, the two cases (2.13) may now be written as: Case I: $\delta/\varepsilon \ll 1$; and Case II: $\delta/\varepsilon = \mathcal{O}(1)$, while the distinction between the subcases **a** and **b** is made by $\varepsilon D/\delta \ll 1$ and $\varepsilon D/\delta = \mathcal{O}(1)$. The leading order quasi-stationary system, to be studied throughout the rest of the paper, may therefore be written, dropping hats and letting overdot denote $d/d\hat{\xi}$, as:

$$\begin{aligned} \dot{u} &= \varepsilon p \\ \dot{p} &= \varepsilon \left[uv^2 - \varepsilon Dc(t)p - \varepsilon \delta \left(1 - \frac{\delta}{\varepsilon}u \right) \right] \\ \dot{v} &= q \\ \dot{q} &= -uv^2 + v - \varepsilon^2 c(t)q. \end{aligned} \quad (4.6)$$

Remark 4.1. ε^2 and δ^2 here are the parameters λ and γ identified in [12]. Note, however that the δ in [12] differs from the δ here. Also, in [12], $\lambda\gamma = 1$ or close to 1, while here $\varepsilon^2\delta^2 \ll 1$.

4.2 Dynamics on the slow manifold

In system (4.6) with any value of ε , the plane $\mathcal{M} \equiv \{(u, p, v, q) | v, q = 0\}$ is invariant under the flow of (4.6), just as was the case in the ODE for stationary solutions as observed in [2]. The presence of this manifold enables us to decompose the dynamics of the system naturally into a slow part (on \mathcal{M}) and a fast part (off of \mathcal{M}). The dynamics on \mathcal{M} is given by the reduced slow system, and this system is linear:

$$\dot{u} = \varepsilon p, \quad \dot{p} = -\varepsilon^2 Dc(t)p - \varepsilon^2 \delta \left(1 - \frac{\delta}{\varepsilon} u\right). \quad (4.7)$$

The homogeneous steady state ($U = 1, V = 0$) corresponds to the saddle fixed point $S = (u = \varepsilon/\delta, p = 0, v = 0, q = 0)$ on the manifold \mathcal{M} . Therefore, there is one major difference between Cases **I** and **II** that manifests itself already, namely the u component of S satisfies $u \gg 1$ in Case **I**, whereas $u = \mathcal{O}(1)$ in Case **II**. See Figure 5.

Exploring further, the eigenvalues of the reduced slow system at S are:

$$\lambda_{\pm} = -\frac{\varepsilon^2 Dc}{2} \pm \delta \varepsilon \sqrt{1 + \frac{\varepsilon^2 D^2 c^2}{4\delta^2}}. \quad (4.8)$$

Hence, the restricted stable and unstable manifolds of S are the lines

$$W^S(S)|_{\mathcal{M}} \equiv \ell^S : p = \frac{\lambda_+}{\varepsilon} \left(u - \frac{\varepsilon}{\delta}\right), \quad W^U(S)|_{\mathcal{M}} \equiv \ell^U : p = \frac{\lambda_-}{\varepsilon} \left(u - \frac{\varepsilon}{\delta}\right). \quad (4.9)$$

As we show now on a case-by-case basis, these formulae reveal that in Case **I**, the lines ℓ^S and ℓ^U are asymptotically vertical, whereas they have a much smaller (albeit still $\mathcal{O}(1/\varepsilon)$) slope in Case **II**. In addition, we will see that, in subcase **a**, the lines ℓ^S and ℓ^U are symmetric about the u axis, while they are asymmetrically disposed about the u axis in subcase **b**. Overall, there will therefore be four geometrically distinct combinations, see Figure 5.

In Case **Ia**, *i.e.*, when $\delta/\varepsilon \ll 1$ and $\varepsilon D/\delta \ll 1$, we find:

$$\lambda_{\pm} = \pm \varepsilon \delta + \text{h.o.t.}, \quad (4.10)$$

so that the restricted stable and unstable manifolds of S are the lines

$$W^S(S)|_{\mathcal{M}} \equiv \ell^S : p = \varepsilon - \delta u + \text{h.o.t.}, \quad \text{and} \quad W^U(S)|_{\mathcal{M}} \equiv \ell^U : p = -\varepsilon + \delta u + \text{h.o.t.} \quad (4.11)$$

These lines are asymptotically vertical in the $p - u$ plane in the region where $u = \mathcal{O}(1)$ when $\delta/\varepsilon \ll 1$, see Figure 5a. Moreover, ℓ^U and ℓ^S are symmetric with respect to the u axis.

In Case **Ib**, *i.e.*, when $\delta/\varepsilon \ll 1$ but now $\varepsilon D/\delta = \mathcal{O}(1)$, all of the terms in the expression (4.8) for the eigenvalues are of leading order. Let $\gamma \equiv \varepsilon D/\delta$ so that $\gamma = \mathcal{O}(1)$. Then, (4.8) yields:

$$\lambda_{\pm} = \varepsilon \delta \tilde{\lambda}_{\pm} = \varepsilon \delta \left[-\frac{1}{2} \gamma c \pm \sqrt{1 + \frac{1}{4} \gamma^2 c^2} \right]. \quad (4.12)$$

Thus, ℓ^S and ℓ^U are given exactly by:

$$p = -\tilde{\lambda}_{\pm} (\varepsilon - \delta u), \quad (4.13)$$

and the first term is the leading order term when $u = \mathcal{O}(1)$ because of the assumption that $\delta/\varepsilon \ll 1$. We therefore note that ℓ^S and ℓ^U are vertical lines to leading order for u of $\mathcal{O}(1)$. However, they are no longer symmetrically disposed about the u -axis due to the difference in the magnitudes of $\tilde{\lambda}_\pm$. This complicates the analysis considerably, as we show in subsection 6.1.

In Case **IIa**, the saddle fixed point is only located an $\mathcal{O}(1)$ distance from the origin along the u axis, since $\delta/\varepsilon = \mathcal{O}(1)$. Hence, the lines ℓ^S and ℓ^U have much smaller slope ('only $\mathcal{O}(1/\varepsilon)$ ') than in Case **I**. In addition, since $\varepsilon D/\delta \ll 1$ here, these lines are again symmetrically disposed about the u axis. Set $\sigma = \delta/\varepsilon$, so that σ is an $\mathcal{O}(1)$ parameter. They are given by

$$p = \pm\varepsilon(1 - \sigma u). \quad (4.14)$$

Finally in going to Case **IIb**, we see that the lines become asymmetric about the u axis. In both subcases **IIa** and **IIb**, there are saddle node bifurcations of the modulated pulse solutions.

Remark 4.2. We do not pay any attention to Case **IIb** in this paper. This is in essence a co-dimension two case that can be studied by combining cases **Ib** and **IIa**, which are represented by the curves \mathcal{C}_{SN} and \mathcal{C}_{TW} , respectively, in Figure 3. Moreover, the combination of $\delta/\varepsilon = \mathcal{O}(1)$ and of $\varepsilon D/\delta = \mathcal{O}(1)$ implies that $D = \mathcal{O}(1)$. Hence, $\mathcal{C}_{\text{SN}} \cap \mathcal{C}_{\text{TW}} = \emptyset$ in Figure 3 since there $D \ll 1$. The case $D = \mathcal{O}(1)$ is of little interest in the light of the stability analysis of Section 7 (see Remark 7.2).

5 Geometric construction of slowly-modulated two pulse solutions

In this section, we construct slowly-modulated two pulse solutions in Case **Ia**. We will use an extension of the geometric method presented in [2] to give an existence proof. The geometric method will also be applied to cases **Ib** and **IIa** in Section 6. In subsections 5.1 and 5.2, we briefly describe the geometry of the fast system when $\varepsilon = 0$ and when $0 < \varepsilon \ll 1$, respectively. We identify the crucial 'take off' and 'touch down' curves in subsection 5.3, geometrically hook up the fast and slow segments of the modulating two pulse solutions in subsection 5.4, and derive the ODE for $c(t)$ in subsection 5.5. Finally, in subsection 5.6, we establish the validity of the quasi-stationary approximation used throughout this work.

5.1 The fast subsystem when $\varepsilon = 0$

The fast subsystem is obtained from (4.6) by noting that u and p remain constant when $\varepsilon = 0$:

$$\dot{v} = q, \quad \dot{q} = -uv^2 + v. \quad (5.1)$$

This reduced fast subsystem is Hamiltonian for each constant u , with $K = q^2/2 + uv^3/3 - v^2/2$. For each positive u , the phase portrait of (5.1) has a center equilibrium at $(\frac{1}{u}, 0)$ and a saddle equilibrium at $(0, 0)$ that possesses an orbit homoclinic to it, given by:

$$v_0(\xi; u) = \frac{3}{2u} \operatorname{sech}^2\left(\frac{\xi}{2}\right) \quad \text{and} \quad q_0(\xi; u) = \dot{v}_0, \quad (5.2)$$

where v_0 here differs slightly from \hat{v}_0 used in Sections 2 and 3. See also Figure 3a in [2].

Let \mathcal{M}_0 denote the two-dimensional plane $\mathcal{M}_0 \equiv \{(u, p, v, q) \mid v, q = 0\}$ obtained in the $\varepsilon = 0$ limit. It coincides with \mathcal{M} , and the subscript just reminds us that $\varepsilon = 0$ in this subsection. That the origin ($v = 0, q = 0$) is a saddle point of the reduced fast system for each positive value of the constant u immediately implies that \mathcal{M}_0 is an invariant manifold and that it is normally hyperbolic. Over each point $(u, p, 0, 0)$ on \mathcal{M}_0 there are one-dimensional fast stable and unstable fibers; these correspond precisely to the local stable and unstable manifolds of the saddle point ($v = 0, q = 0$) of the fast subsystem. Hence, when $u > 0$, the manifold \mathcal{M}_0 has three-dimensional stable and unstable manifolds, $W^S(\mathcal{M}_0)$ and $W^U(\mathcal{M}_0)$, that are simply the unions of the above one-dimensional fibers over the two-dimensional set of base points $(u, p, 0, 0)$ on \mathcal{M}_0 . Moreover, since these local manifolds coincide in the fast subsystem to form the homoclinic orbit given by (5.2), it follows directly that each point on \mathcal{M}_0 is connected to itself by a homoclinic orbit, and that the manifold \mathcal{M}_0 possesses a three-dimensional homoclinic manifold $W(\mathcal{M}_0)$.

5.2 Persistent fast connections

When $0 < \varepsilon \ll 1$ in (4.6), Fenichel theory [10] implies that the stable and unstable manifolds of \mathcal{M} present in the $\varepsilon = 0$ system persist as three-dimensional, C^r smooth stable and unstable manifolds, $W^U(\mathcal{M})$ and $W^S(\mathcal{M})$. See also Theorem 3 of [14]. However, the branches of these manifolds that coincided when $\varepsilon = 0$ generally no longer do so, and intersect each other in two-dimensional surfaces. In these intersections lie the only one-pulse orbits biasymptotic to \mathcal{M} .

In this subsection, we employ a Melnikov method to detect these intersections. System (4.6) is of the type to which Robinson's extension of the Melnikov method applies, see [26] as well as the other references cited in [2]. Let $(u(\xi), p(\xi), v(\xi), q(\xi))$ represent a solution of (4.6) that passes through the point $(u_0, p_0, v(0), 0)$ when $\xi = 0$. The splitting distance between the manifolds $W^U(\mathcal{M})$ and $W^S(\mathcal{M})$ can be measured in the hyperplane $\{q = 0\}$, which is the hyperplane transverse to $W(\mathcal{M})$ and is spanned by the three vectors $(1, 0, 0, 0)$, $(0, 1, 0, 0)$, and the unit normal $\hat{n} = (0, 0, 1, 0)$ to $W(\mathcal{M}_0)$. The distance is:

$$\Delta K(u_0, p_0; a, b, c) \equiv \int_{-\infty}^{\infty} \dot{K}(v(\xi), q(\xi); u(\xi), p(\xi)) d\xi, \quad (5.3)$$

as $\varepsilon \rightarrow 0^+$, and the integrand is given by a straightforward computation: $\dot{K} = \frac{1}{3}\varepsilon p v^3 - \varepsilon^2 c(t) q^2$.

Solutions $(u(\xi), p(\xi), v(\xi), q(\xi))$ of (4.6) on the perturbed stable and unstable manifolds $W^S(\mathcal{M})$ and $W^U(\mathcal{M})$ can be expanded in powers of the small parameter ε :

$$\begin{aligned} u(\xi) &= u_0 + \varepsilon u_1(\xi) + \varepsilon^2 u_2(\xi) + \text{h.o.t} & p(\xi) &= p_0 + \varepsilon p_1(\xi) + \varepsilon^2 p_2(\xi) + \text{h.o.t} \\ v(\xi) &= v_0(\xi; u_0) + \varepsilon v_1(\xi) + \varepsilon^2 v_2(\xi) + \text{h.o.t} & q(\xi) &= q_0(\xi; u_0) + \varepsilon q_1(\xi) + \varepsilon^2 q_2(\xi) + \text{h.o.t}, \end{aligned} \quad (5.4)$$

as $\varepsilon \rightarrow 0$, where $v_0(\xi; u_0)$ and $q_0(\xi; u_0)$ are the unperturbed homoclinic solutions (5.2). Solutions on $W^U(\mathcal{M})$ are represented by expansions valid on the semi-infinite time interval $(-\infty, 0]$, and solutions on $W^S(\mathcal{M})$ are represented by expansions valid on the semi-infinite time interval $[0, \infty)$.

We fix initial conditions on the curves $W^S(\mathcal{M}) \cap \{q = 0\}$ and $W^U(\mathcal{M}) \cap \{q = 0\}$ whose v coordinates lie in a neighborhood of $3/(2u)$. We assume that $u(0) = u_0$ and $u_j(0) = 0$ for $j \geq 1$: the initial conditions $p_0, p_j(0)$ and $v_j(0)$ ($j \geq 1$) are then determined as functions of u_0 by the condition that the orbit of $(u(\xi), p(\xi), v(\xi), q(\xi))$ lies in the transverse intersection of $W^S(\mathcal{M})$ and $W^U(\mathcal{M})$. We label such an orbit $\Gamma(\xi; x_0)$, where $x_0 = (u_0, p(0), v(0), 0)$.

One observes straightaway that $p_0 = 0$, since the p coordinates of all points on ℓ^S and ℓ^U with u coordinate of size $\mathcal{O}(1)$ are at most $\mathcal{O}(\varepsilon)$ in magnitude, see (4.11), and hence the only way for the initial conditions x_0 to lead to an orbit that is either forward or backward asymptotic to S is if $p(0) = \mathcal{O}(\varepsilon)$. Also, the first-order corrections of u and p are found by substituting (5.4) into (4.6):

$$u_1(\xi) \equiv 0, \quad p_1(\xi) = \int_0^\xi u_0 v_0^2(s) ds + p_1(0). \quad (5.5)$$

Hence, the integral in $p_1(\xi)$ is an odd function of ξ , because $v_0(\xi)$ is an even in ξ . Plugging these expansions into \dot{K} and (5.3) and using odd-even properties yields:

$$\Delta K(u_0, p(0); a, b, c(t)) = \varepsilon^2 \left[\frac{1}{3} p_1(0) \int_{-\infty}^{\infty} v_0^3(\xi) d\xi - c(t) \int_{-\infty}^{\infty} q_0^2(\xi) d\xi \right] + \text{h.o.t} \quad (5.6)$$

Therefore, using (5.2), the zero set of ΔK is given to leading order by the line

$$p = \frac{1}{2} \varepsilon c u, \quad (5.7)$$

where we recall u is assumed $\mathcal{O}(1)$. Hence, there exist initial conditions $x_0 = (u_0, p(0), v(0), 0)$ such that the orbits $\Gamma(\xi; x_0)$ through these points are biasymptotic to \mathcal{M} if the u and p coordinates of the initial conditions chosen above are related to leading order as in (5.7), with $p = \mathcal{O}(\varepsilon)$. Also, as $c \rightarrow 0^+$, the zero line of ΔK approaches the vertical, see Remark 5.2.

In order to quantify the influence of the fast field on the u - and p -coordinates of a solution in $W^U(\mathcal{M}) \cap W^S(\mathcal{M})$ during its excursion through the fast field, we define

$$\Delta p(u_0, p(0); a, b, c(t)) \equiv \int_{-\infty}^{\infty} \dot{p} d\xi \quad \text{and} \quad \Delta u(u_0, p(0); a, b, c(t)) \equiv \int_{-\infty}^{\infty} \dot{u} d\xi.$$

Before evaluating these expressions, we note that $\Delta K = \mathcal{O}(\varepsilon^2)$ implies $|v(0) - v_0| = \mathcal{O}(\varepsilon^2)$. Hence, $v_1(\xi) \equiv 0$, since v_1 is the solution of a second-order equation with initial conditions $v_1(0), \dot{v}_1(0) = 0$. Straightforward computations now give:

$$\Delta p = \varepsilon \int_{-\infty}^{\infty} \left(u(\xi) v^2(\xi) + \text{h.o.t} \right) d\xi = \varepsilon \int_{-\infty}^{\infty} u_0 v_0^2(\xi) d\xi + \text{h.o.t} = \varepsilon \frac{6}{u_0} + \text{h.o.t.}, \quad (5.8)$$

where we have also used (4.6), (5.5) and the fact that $\int_{-\infty}^{\infty} v_0^2(\xi) d\xi = 6/u_0^2$.

Finally, to determine the change in u during the fast field, we again use the fact that we will only study $\Delta u(u_0, p(0))$ for values of $(u_0, p(0))$ in the neighborhood of the $\Delta K = 0$ line (5.7). As above, therefore, $p(\xi) = \mathcal{O}(\varepsilon)$ on the time interval under consideration, which implies that the change in u during the excursion in the fast field is of higher order:

$$\Delta u \sim \varepsilon^2. \quad (5.9)$$

5.3 Take off and touch down curves

There are two other curves on \mathcal{M} that play a crucial role in the analysis. These are obtained as follows. The first intersection of $W^S(\mathcal{M})$ and $W^U(\mathcal{M})$ in the hyperplane $\{q = 0\}$ is given by (5.7)

to leading order. This intersection is a one-dimensional curve in the two-dimensional manifold $W^S(\mathcal{M}) \cap W^U(\mathcal{M})$. Through any point x_0 on this curve $W^S(\mathcal{M}) \cap W^U(\mathcal{M}) \cap \{q = 0\}$ there is an orbit $\Gamma(\xi; x_0)$ which approaches \mathcal{M} for ‘large’ $|\xi|$. More precisely, the Fenichel theory [10] implies that for any $\Gamma(\xi; x_0)$ there are two orbits $\Gamma_{\mathcal{M}}^+ = \Gamma_{\mathcal{M}}^+(\xi; x_0^+) \subset \mathcal{M}$ and $\Gamma_{\mathcal{M}}^-(\xi; x_0^-) \subset \mathcal{M}$, respectively (where $\Gamma^+(0; x_0^+) = x_0^+ \in \mathcal{M}$), such that $\|\Gamma(\xi; x_0) - \Gamma_{\mathcal{M}}^+(\xi; x_0^+)\|$ is exponentially small for $\xi > 0$ where $t \geq \mathcal{O}(\frac{1}{\varepsilon})$ and $\|\Gamma(\xi; x_0) - \Gamma_{\mathcal{M}}^-(\xi; x_0^-)\|$ is exponentially small for $-\xi \geq \frac{K}{\varepsilon} > 0$. Thus,

$$d(\Gamma(\xi; x_0), \mathcal{M}) = \mathcal{O}\left(e^{-\frac{k}{\varepsilon}}\right) \quad \text{for } |\xi| \geq \mathcal{O}\left(\frac{1}{\varepsilon}\right) \quad \text{or larger}$$

for some $k > 0$, and $\Gamma_{\mathcal{M}}^\pm(\xi; x_0^\pm)$ determine the behavior of $\Gamma(\xi; x_0)$ near \mathcal{M} . These orbits on \mathcal{M} are the orbits of the base points of the fast stable and unstable fibers in whose intersection Γ lies.

Therefore, we define the curves $T_o \subset \mathcal{M}$ (take off) and $T_d \subset \mathcal{M}$ (touch down) as

$$T_o = \cup_{x_0} \{x_0^- = \Gamma_{\mathcal{M}}^-(0; x_0^-)\}, \quad \text{and} \quad T_d = \cup_{x_0} \{x_0^+ = \Gamma_{\mathcal{M}}^+(0; x_0^+)\}, \quad (5.10)$$

where the unions are over all x_0 in $W^S(\mathcal{M}) \cap W^U(\mathcal{M}) \cap \{q = 0\}$. T_o , respectively T_d , is the collection of base points of all of the fibers in $W^U(\mathcal{M})$ (respectively $W^S(\mathcal{M})$) that lie in the transverse intersection of $W^U(\mathcal{M})$ and $W^S(\mathcal{M})$.

The locations of T_o and T_d can be obtained explicitly by determining the relations between $x_0 = (u_0, p(0), v(0), 0)$ and $x_0^\pm = (u_0^\pm, p_0^\pm, 0, 0)$. The accumulated changes in p of $\Gamma(t)$ during the backward and forward (half-circuit) excursions through the fast field are measured by $\int_{-\infty}^0 \dot{p} d\xi$ and $\int_0^\infty \dot{p} d\xi$, respectively. The changes in p of $\Gamma^\pm(t)$ during the same period of time can be neglected, to leading order, since $\dot{p} = \mathcal{O}(\varepsilon^3)$ on \mathcal{M} by (4.6). Formulae (4.6) and (5.9) imply $u_0 = u_0^\pm$ to leading order. Therefore, by the same calculations that led to (5.7) and (5.8), one finds to leading order:

$$T_o : p = \frac{1}{2}\varepsilon \left[cu - \frac{6}{u} \right], \quad T_d : p = \frac{1}{2}\varepsilon \left[cu + \frac{6}{u} \right]. \quad (5.11)$$

5.4 The right-moving pulse with slowly-changing $c(t)$: hooking up the slow and fast segments

In this subsection, we construct instantaneous (fixed t) snapshots of the right-moving pulse solution on $x \geq 0$. As stated above, at any instant of time t , this solution consists of three segments, and we start with the slow segment to the right of the peak. These instantaneous t snapshots will then be put together in the following subsection in a self-consistent fashion determined by how the wave speed $c(t)$ slowly changes in time. We remark that we reintroduce hats on the independent variable ξ where appropriate in these last subsections.

For instantaneous wave speeds satisfying $0 < c(t) < 1/6$, the curve T_d on \mathcal{M} intersects the line ℓ^S in two distinct points. The leading order analysis in (4.11) and (5.11) directly yields that the upper and lower intersection points are $(u_\pm, p_R(u_\pm))$, respectively, where

$$u_\pm = \frac{1}{c(t)} \left(1 \pm \sqrt{1 - 6c(t)} \right), \quad (5.12)$$

and $p_R(u_\pm)$ is given to leading order by the first term in (4.11)(a). See Figure 6. We note that $du_-/dc > 0$ for all $c > 0$. This leading order analysis also identifies the critical (maximum) wave

speed as $c(t) = 1/6$. At this $c(t)$ value, the two curves are tangent, and it represents to leading order the initial value of the wave speed of the pulses with slowly-decreasing wave speed.

To leading order, the right slow segment we are interested in is given by the orbit along that segment of ℓ^S from $u = u_-$ to $u = \varepsilon/\delta$. This right slow segment satisfies the asymptotic condition $U \rightarrow 1$ because the solution on ℓ^S approaches S , *i.e.*, $u \rightarrow \varepsilon/\delta$ and $p \rightarrow 0$. See Figure 6. The v and q coordinates are exponentially small, and hence zero to leading order and to all orders.

At the intersection point $(u_-, p_R(u_-))$, the right slow segment is hooked up to the fast segment. This fast segment is given to leading order by the homoclinic orbit (5.2) of the fast reduced system (5.1) with $\varepsilon = 0$, where the constant u , and hence also the u component of the initial condition, are fixed at u_- . See Figure 6. That these solution segments can be hooked up smoothly in this fashion for the full system with $0 < \varepsilon \ll 1$ is justified by the fact that, for $c < 1/6$, the curves T_d and ℓ^S intersect transversely on \mathcal{M} at $(u_-, p_R(u_-))$, and hence the geometric singular perturbation theory of Fenichel may be applied, see [10] and [14].

The backward asymptotic ($\hat{\xi} \rightarrow -\infty$) limit set of the fast homoclinic pulse is the point $(u_-, p_L(u_-))$ on \mathcal{M} . We use (4.11) and (5.11) to compute to leading order:

$$p_L(u_-) = p_R(u_-) - \Delta p(u_-) = \varepsilon \left(1 - \frac{6}{u_-} \right) = -\varepsilon \sqrt{1 - 6c(t)}. \quad (5.13)$$

See Figure 6. The point $(u_-, p_L(u_-))$ lies on the take off curve T_o , and the result (5.13) expresses the fact that the jump from T_o (namely $(u_-, p_L(u_-))$) to T_d (namely $(u_-, p_R(u_-))$) during the fast segment is given to leading order by the accumulated change $\Delta p(u_-)$ in p , where of course u stays constant to a sufficiently high order by (4.22). In addition, for $0 < c(t) < 1/6$, the point $(u_-, p_L(u_-))$ lies to the right of the line ℓ^U , inside the triangle formed by these lines and the p -axis, whereas it lies on ℓ^U for $c = 0$, see [2].

The identification of $(u_-, p_L(u_-))$ completes the specification of the fast segment, and it is precisely at this point that we hook up the fast segment to the left slow segment. To leading order, the left slow solution is the segment of a hyperbolic cosine orbit on \mathcal{M} (inside the triangle) between the points $(u_{\max}, 0)$ and $(u_-, p_L(u_-))$. See Figure 6. The u component is given to leading order by:

$$u(\hat{\xi}) = \frac{\varepsilon}{\delta} + \mathcal{A}e^{\varepsilon\delta\hat{\xi}} + \mathcal{B}e^{-\varepsilon\delta\hat{\xi}}, \quad (5.14)$$

where the unknown coefficients are determined by imposing the two given boundary conditions. Without loss of generality, since the ODE system is autonomous in ξ (and $\hat{\xi}$), we are free to choose the parametrization such that $(u(\xi), p(\xi))|_{\xi=0} = (u_-, p_L(u_-))$. Hence, we impose $u(\xi = 0) = u_-$ and $\frac{du}{d\xi}(\xi = 0) = \varepsilon p_L(u_-)$, which yields the conditions:

$$\mathcal{A} + \mathcal{B} = -\frac{\varepsilon}{\delta} + \mathcal{O}(1) \quad \text{and} \quad \mathcal{A} - \mathcal{B} = -\frac{\varepsilon}{\delta} \sqrt{1 - 6c(t)} + \mathcal{O}(1).$$

Note that we used that $u_- = \mathcal{O}(1)$ by (5.12) and that $p_L(u_-) = \mathcal{O}(\varepsilon)$ by (5.13), while $\varepsilon/\delta \gg 1$. Therefore, letting $H \equiv \sqrt{1 - 6c(t)}$, we obtain:

$$\begin{aligned} u(\hat{\xi}) &= \frac{\varepsilon}{2\delta} \left[2 - (1 + H)e^{\varepsilon\delta\hat{\xi}} + (H - 1)e^{-\varepsilon\delta\hat{\xi}} \right] + \text{h.o.t} \\ p(\hat{\xi}) &= -\frac{\varepsilon}{2} \left[(1 + H)e^{\varepsilon\delta\hat{\xi}} + (H - 1)e^{-\varepsilon\delta\hat{\xi}} \right] + \text{h.o.t.} \end{aligned} \quad (5.15)$$

Thus, the left slow segment satisfies the left boundary condition $du/dx = 0$ at $x = 0$ for our right-moving pulse solution at every instant of time t . In the full system, the hooking up of the left slow segment and the fast segment is justified in the same way as that done for the right slow segment.

Finally, with this explicit solution in hand, we can also explicitly calculate the value of $\hat{\xi}$ at which the slow segment begins, *i.e.*, at which $u(\hat{\xi}) = u_{\max}$ and $p(\hat{\xi}) = 0$. We label this value $\hat{\xi}_{\max}$ and observe that it is negative and that it is equal to $\Gamma(t)$ from Section 3. See Figure 6. In particular, by imposing $p(\hat{\xi}_{\max}) = 0$ in (5.15)(b), one finds to leading order:

$$\hat{\xi}_{\max} = \frac{1}{2\varepsilon\delta} \ln \left(\frac{1-H}{1+H} \right). \quad (5.16)$$

Combining (5.15) and (5.16) yields the expression for u_{\max} , since $u_{\max} = \mathcal{O}(\varepsilon/\delta)$ we unscale (4.2):

$$u_{\max}(t) \stackrel{\text{def}}{=} \frac{\varepsilon}{\delta} U_{\max}(t) = \frac{\varepsilon}{\delta} \left(1 - \sqrt{6\hat{c}(t)} \right), \quad (5.17)$$

thus, $U_{\max}(t) = U(0, t)$, the unscaled value of the solution $U(x, t)$ of (1.1) at $x = 0$ (see Figure 1). Below we will find that $\hat{c}(t) \in (0, 1/6)$, *i.e.* $U_{\max}(t) \in (0, 1)$. These last formulae (5.16) and (5.17) complete our leading order description of the right moving pulse solution on the domain $x \geq 0$ at each instant of time t , with $c(t)$ as yet unknown. The solution on $x \leq 0$ at the same instant of time t is determined by reflecting the solution on $x \geq 0$ across $x = 0$.

Remark 5.1. The above analysis specifies the leading order solution for the right-moving pulse. When $0 < \varepsilon \ll 1$, this solution is in $W^S(\mathcal{M})$ and lies exponentially close to the transverse intersection of the local manifolds $W_{\text{loc}}^U(\mathcal{M})$ and $W_{\text{loc}}^S(\mathcal{M})$. Also, as $\hat{\xi}$ decreases to $\hat{\xi}_{\max}$, the orbit comes exponentially close to \mathcal{M} with exponentially small (but nonzero) V component.

5.5 The ODE for $c(t)$ in Case Ia

In this subsection, we determine the explicit formula for the slow rate of change of $c(t)$. This will complete our existence proof of the full right-moving pulse solution with slowly-decreasing wave speed in Case **Ia**, *i.e.*, in the regime where $\varepsilon D/\delta \ll 1$. In this subsection, we will again put a hat on the variable c where appropriate.

Recall from (4.1) that the traveling wave variable was defined as $\xi = x - \int_0^t c(s) ds$, where ξ and c are unscaled. Plugging in the scalings for ξ and c given by (4.3) and (4.6), respectively, and evaluating at $x = 0$ (*i.e.*, at $\xi = \hat{\xi}_{\max} = -\int_0^t c(s) ds < 0$), one finds:

$$\hat{\xi}_{\max} = \frac{-\varepsilon^2 \delta^2}{D} \int_0^t \hat{c}(s) ds. \quad (5.18)$$

At each fixed instant of time t , this value of $\hat{\xi}_{\max}$ represents precisely the distance between the origin ($x = 0$) and the center of the peak. Moreover, this value (5.18) must agree with (5.16), the value calculated earlier during the geometric construction in the previous subsection. Hence, equating (5.16) and (5.18) results in the following implicit formula for $\hat{c}(t)$:

$$\ln \left(\frac{1 - \sqrt{1 - 6\hat{c}(t)}}{1 + \sqrt{1 - 6\hat{c}(t)}} \right) = \frac{-2\varepsilon^3 \delta^3}{D} \int_0^t \hat{c}(s) ds, \quad (5.19)$$

where we recall that the parameter H introduced there is defined in terms of \hat{c} . Finally, differentiating both sides of (5.19) with respect to t yields the desired ODE:

$$\frac{d\hat{c}}{dt} = \frac{-2\epsilon^3 \delta^3 \hat{c}^2}{D} \sqrt{1 - 6\hat{c}}, \quad (5.20)$$

which is exactly the same as the ODE (3.32) found in Section 3 (use (4.2) and (4.5)). One observes directly that $\hat{c} = 1/6$ is an unstable fixed point and that the existence of this critical maximum value of \hat{c} has a clear geometric origin, namely it is the \hat{c} value at which T_d is tangent to ℓ^S . Also, since $d\hat{c}/dt$ scales as $-\hat{c}^2$ for small \hat{c} , we know \hat{c} decays as $1/t$.

Remark 5.2. The $c = 0$ case is treated explicitly in [2], and one must take into account higher order terms here when analyzing the transition from $c > 0$ to $c = 0$.

Remark 5.3. Using the same procedure employed above, we can also show that the above-type two-pulse solutions with u near u_+ , the second solution in (5.12), in the fast field do not exist. In particular, since $p_R(u_+) = \epsilon$ to leading order, $p_L(u_+) = p_R(u_+) - \Delta p(u_+) = \epsilon[1 - (6/u_+)] = \epsilon H$, where we recall $H = \sqrt{1 - 6c}$. Hence, $p_L(u_+) > 0$ for all $0 \leq c \leq 1/6$, and one cannot hook up the fast jump to a slow (cosh-type) solution that reaches $p = 0$ for some $\hat{\xi}_{\max} < 0$.

5.6 The validity of the quasi-stationary approach

For slowly-modulated two-pulse solutions (U, V) of (1.1), the key ingredients in the quasi-stationary approach used throughout this paper are: (i) the decomposition into a part traveling to the right and a part traveling to the left; (ii) the introduction of a traveling coordinate ξ in which the speed c is allowed to vary slowly in time (3.32), (5.20); and (iii) the assumption that the explicit time derivative terms $\partial U/\partial t$ and $\partial V/\partial t$ are small and hence can be neglected to leading order. As a result of these assumptions, the equations (1.1) reduced to a system of two second-order ordinary differential equations for $u(\xi)$ and $v(\xi)$, in which the wave speed $c(t)$ appeared as a slowly-varying parameter. Also, the decomposition imposed boundary conditions at $x = 0$, and in turn both the analytical and the geometrical approaches used these boundary conditions to determine the ODE for $c(t)$. In this subsection, the validity of this approach is analyzed.

It is essential to begin by observing that a smooth solution of the full PDE (1.1) must satisfy

$$\left. \begin{aligned} \lim_{x \uparrow 0} \frac{\partial^k}{\partial x^k} U(x, t) &= \lim_{x \downarrow 0} \frac{\partial^k}{\partial x^k} U(x, t) \\ \lim_{x \uparrow 0} \frac{\partial^k}{\partial x^k} V(x, t) &= \lim_{x \downarrow 0} \frac{\partial^k}{\partial x^k} V(x, t) \end{aligned} \right\} \text{ for all } t \geq 0, k \geq 0. \quad (5.21)$$

Moreover, the reversibility symmetry of (1.1) implies that all odd derivatives at $x = 0$ vanish (see Figure 1: the two-pulse solution is even as function of x). We now show, however, that the third-order derivative of U at $x = 0$, as well as all odd higher-order spatial derivatives there, are small, but nonzero, for the leading order approximation obtained from the quasi-stationary analysis. In addition, we show that the reintroduction of the explicit (and higher-order) time derivative terms remedies this defect and results in a smooth and consistent solution of the full PDE (1.1).

To leading order, the quasi-stationary approach implies that one assumes $(U(x, t), V(x, t)) = (u(\xi_r(t)), v(\xi_r(t)))$ for $x \geq 0$, and $(U(x, t), V(x, t)) = (u(\xi_l(t)), v(\xi_l(t)))$ for $x \leq 0$, where the traveling coordinates $\xi_{r,l}(t)$ are given by $\xi_r(t) = x - \Gamma(t) = x - \int_0^t c(s) ds$ (for $x \geq 0$) and $\xi_l(t) =$

$x + \Gamma(t)$ (for $x \leq 0$). In this context, the boundary conditions (5.21) for u become

$$\begin{aligned} \frac{\partial^{2m}}{\partial \xi_r^{2m}} u(\xi_r)|_{\xi_r = -\Gamma(t)} &= \frac{\partial^{2m}}{\partial \xi_l^{2m}} u(\xi_l)|_{\xi_l = \Gamma(t)}, \\ \frac{\partial^{2n+1}}{\partial \xi_r^{2n+1}} u(\xi_r)|_{\xi_r = -\Gamma(t)} &= \frac{\partial^{2n+1}}{\partial \xi_l^{2n+1}} u(\xi_l)|_{\xi_l = \Gamma(t)} = 0, \end{aligned} \quad (5.22)$$

for all $m, n \geq 0$ and $t \geq 0$, where only the conditions involving $m, n = 0$ were used in the construction of the two-pulse solutions. Also, the conditions on $v(\xi_{r,l})$ may be ignored here, since v and its derivatives are exponentially small near $x = 0$.

Now, it is a straightforward computation to check that

$$\begin{aligned} \frac{\partial^2}{\partial \xi_r^2} u(-\Gamma(t)) &= \frac{\partial^2}{\partial \xi_l^2} u(\Gamma(t)) = -A(1 - U_{\max}(t)) \\ \frac{\partial^3}{\partial \xi_r^3} u(-\Gamma(t)) &= -\frac{\partial^3}{\partial \xi_l^3} u(\Gamma(t)) = c(t)A(1 - U_{\max}(t)) \neq 0, \end{aligned} \quad (5.23)$$

where $U_{\max}(t) = u(\xi_r)|_{\xi_r = -\Gamma(t)} = u(\xi_l)|_{\xi_l = \Gamma(t)}$, see (5.17). Thus, it follows immediately that, while the first condition in (5.22) is satisfied for $m = 1$, there is a ‘jump’ in the third derivative at $x = 0$ and the second condition in (5.22) is not satisfied for $n = 1$. Specifically, this jump is given by:

$$\Delta \frac{\partial^3 U}{\partial \hat{\xi}^3} = \mathcal{O}\left(\frac{A^2 D^2}{B^3}\right) = \mathcal{O}(\varepsilon^4 \delta D) \ll 1, \quad (5.24)$$

where we have used the proper scales for the spatial variable $\hat{\xi}_{r,l}$ (4.2) and the wave speed c (4.2), as well as (4.5). Moreover, there are jumps in all of the higher-order odd derivatives at $x = 0$ as well. Therefore, the leading order approximation obtained from the quasi-stationary analysis has a defect in that it does not give a smooth solution of the PDE (1.1). Also, this defect is inherent in the leading order approximation, since the pulses are determined up to all orders in the perturbation expansion by the $m, n = 0$ boundary conditions (5.22) applied to the ODE (4.6), and hence there is no ‘freedom’ left in the ODE reduction to satisfy the other boundary conditions with $m > 0, n > 0$.

To remedy this defect in the leading-order quasi-stationary approximation we consider the higher-order the explicit time derivative terms. Therefore, we introduce a *slow* time variable:

$$\tau = \left(\frac{A}{B}\right)^{\frac{3}{2}} \sqrt{Dt} = \frac{\varepsilon^3 \delta^3}{D} t. \quad (5.25)$$

Also, we look for two-pulse solutions of (1.1) that depend on both ξ_r (or ξ_l) and τ :

$$\begin{aligned} (U(x, t), V(x, t)) &= (U(\xi_r(\tau), \tau), V(\xi_r(\tau), \tau)) \quad \text{for } x \geq 0 \\ (U(x, t), V(x, t)) &= (U(\xi_l(\tau), \tau), V(\xi_l(\tau), \tau)) \quad \text{for } x \leq 0. \end{aligned} \quad (5.26)$$

The slow time variable τ makes it explicit that (U, V) evolves on the same (slow) time scale as c and U_{\max} (see (5.17)), and we note that the choice (5.25) can also be obtained by assuming a general scaling for τ and then determining its ‘significant degeneration’, see [6].

Working explicitly on the domain $x > 0$ and with the right moving pulse (*i.e.*, using $\xi = \xi_r$), the boundary condition at $x = 0$ is:

$$U(-\Gamma(\tau), \tau) \stackrel{\text{def}}{=} U_{\max}(\tau), \quad \text{and} \quad U_\xi(-\Gamma(\tau), \tau) = 0 \quad \text{for all } \tau \geq 0. \quad (5.27)$$

So, now, assuming that $V(\xi(\tau), \tau)$ is negligible near $x = 0$ (like $v(\xi(\tau))$ in the ODE) and that the $U_{\max}(\tau)$ is the same (to leading order) as the one determined by the ODE approach, one finds:

$$\frac{\partial}{\partial \tau} U(\xi_r = -\Gamma, \tau) = \frac{d}{d\tau} U_{\max}(\tau), \quad (5.28)$$

see (5.20) and (5.17) for the explicit leading order expression, and a similar expression can be obtained for the left moving pulse.

Remark 5.4. Of course, at this stage, one still has to check for consistency whether the explicit dependence of U, V on τ only has a higher order influence on the behavior of $U(\xi(\tau), \tau)$ and $V(\xi(\tau), \tau)$ compared to $u(\xi(\tau))$ and $v(\xi(\tau))$ (for all x , not only near $x = 0$).

With the formula (5.28) in hand, one readily verifies that the first boundary condition in (5.22) is still satisfied with $m = 1$. In particular, by evaluating all of the terms in the PDE for the U components of the solutions (5.26) at $\xi_r = -\Gamma(t)$ and at $\xi_l = \Gamma(t)$ and by neglecting terms involving $V(\xi, \tau)$, $V_\tau(\xi, \tau)$, and their derivatives with respect to ξ which are all exponentially small in a neighborhood of $x = 0$, we find:

$$\frac{\partial^2}{\partial \xi_r^2} U(-\Gamma(\tau), \tau) = \frac{\partial^2}{\partial \xi_l^2} U(\Gamma(\tau), \tau) = \frac{d}{d\tau} U_{\max}(\tau) - A(1 - U_{\max}(\tau)). \quad (5.29)$$

Finally, by differentiating the PDE for U once with respect to ξ and again neglecting exponentially small terms, we deduce the desired result:

$$\frac{\partial^3}{\partial \xi_r^3} U(-\Gamma(\tau), \tau) = \frac{\partial^3}{\partial \xi_l^3} U(\Gamma(\tau), \tau) = 0, \quad (5.30)$$

since differentiation of the second condition in (5.27) with respect to τ and use of the chain rule reveals that $U_{\xi_r \tau}(-\Gamma(\tau), \tau) = c(\tau) U_{\xi_r \xi_r}(-\Gamma(\tau), \tau)$, and a similar equality holds for the solution on $x < 0$. Similarly, one shows that all of the higher order derivatives of $(U(\xi_r(\tau), \tau), V(\xi_r(\tau), \tau))$ and $(U(\xi_l(\tau), \tau), V(\xi_l(\tau), \tau))$ are equal at $x = 0$, *i.e.*, that $(U(\xi_{r,l}(\tau), \tau), V(\xi_{r,l}(\tau), \tau))$ satisfies the boundary conditions (5.21), (5.22) for all $m, n \geq 0$. Therefore, with the higher-order terms included, the quasi-stationary approximation (5.26) is smooth at $x = 0$ to all orders.

We conclude this section by showing that the improved quasi-stationary approximation is *consistent*, *i.e.*, we show that the introduction of the explicit temporal behavior does not influence the ODE methods of the previous sections to leading order. In particular, we scale $(U(\xi(\tau), \tau), V(\xi(\tau), \tau))$ into $(\hat{U}(\hat{\xi}(\tau), \tau), \hat{V}(\hat{\xi}(\tau), \tau))$, precisely as in (4.2), and we use (4.5) and (5.25) to write the PDE for (\hat{U}, \hat{V}) in the form of the ODE for (\hat{u}, \hat{v}) (4.6) associated to the leading order quasi-stationary approximation (for $\xi = \xi_r$, *i.e.*, $x \geq 0$):

$$\begin{aligned} \hat{U}_{\hat{\xi}} &= \varepsilon \hat{P} \\ \hat{P}_{\hat{\xi}} &= \varepsilon \left[\hat{U} \hat{V}^2 - \varepsilon D \hat{c}(\tau) \hat{P} - \varepsilon \delta \left(1 - \frac{\delta}{\varepsilon} \hat{U} + D \hat{U}_\tau \right) \right] \\ \hat{V}_{\hat{\xi}} &= \hat{Q} \\ \hat{Q}_{\hat{\xi}} &= -\hat{U} \hat{V}^2 + \hat{V} - \varepsilon^2 \hat{c}(\tau) \hat{Q} + \varepsilon^3 \delta \hat{V}_\tau. \end{aligned} \quad (5.31)$$

The invariant slow manifold \mathcal{M} of the ODE (4.6) persists, along with its fast stable and unstable manifolds, for this system. Moreover, since the manifolds $W^S(\mathcal{M})$ and $W^U(\mathcal{M})$ intersect transversely in the phase space of the original ODE, the smallness of the coefficients in front of the \hat{U}_τ

and the \hat{V}_τ terms implies that they continue to intersect in (5.31). Hence, the geometric singular perturbation analysis by which the traveling pulses are constructed is not influenced by these terms, and the ‘PDE contributions’ \hat{U}_τ and \hat{V}_τ cannot have a leading order effect on the analysis. Note, however, that the term $D\hat{U}_\tau$ will have a leading order effect on the flow on \mathcal{M} when $D \geq \mathcal{O}(1)$. As a consequence, the improved quasi-stationary approach will (a priori) only be consistent when we impose that $D \ll 1$. We will find in Section 7 that the stationary 1-pulses can only be stable when $D \ll 1$. Since the modulated two-pulses solutions converge to two copies of these stationary 1-pulses ($c \rightarrow 0$ if $t \rightarrow \infty$), there is no reason to expect that the case $D \geq \mathcal{O}(1)$ will be relevant in the analysis the two-pulse solutions.

Thus, the improved quasi-stationary approach is consistent: the leading order behavior of (U, V) is given by the solution (u, v) determined by the ODE dynamics (and thus it follows for instance that $V(x, t)$ is exponentially small near $x = 0$) and the transition from $x \leq 0$ to $x \geq 0$ is smooth. The validity of the improved quasi-stationary approximation can now be proved by a combination of the transversality results of the geometric analysis (see [10], [14]) and by explicitly showing that \hat{U}_τ and \hat{V}_τ are both $\mathcal{O}(1)$. We do not consider the details any further here.

6 Geometric constructions of two-pulse solutions: Cases Ib & IIa

6.1 Case Ib: $\varepsilon D/\delta = \mathcal{O}(1)$: the boundary of the existence domain for the slowly modulated waves

In this subsection, we study the existence of slowly-modulated two pulse solutions in Case **Ib**, *i.e.*, in that part of parameter space where $\delta/\varepsilon \ll 1$ but $\varepsilon D/\delta = \mathcal{O}(1)$. We will find that the slowly-modulated solutions exist only for $\varepsilon D/\delta < 3$, and that there exist critical *constant* values of $c \neq c(t)$ for which ‘classical’ traveling waves exist. These values of c will later be interpreted as critical points of the ODE for $c(t)$.

A modulated traveling wave corresponds to an orbit that is asymptotically close to ℓ^U for $\xi \ll -1$ and to ℓ^S for $\xi \gg 1$. These orbits lie exponentially close to intersections $\ell^U \cap T_o$ and $\ell^S \cap T_d$ with the same u -coordinates (since, u does not change (to leading order) after one circuit through the fast field (5.9)). Note that T_o and T_d are still given by (5.11). Thus, combining (5.11) with (4.13), we obtain:

$$-\tilde{\lambda}_- = \frac{1}{2}[cu - \frac{6}{u}], \quad -\tilde{\lambda}_+ = \frac{1}{2}[cu + \frac{6}{u}]. \quad (6.1)$$

By (4.12), this immediately yields that either $c = 0$ or $u = \gamma$ (recall that $\gamma = \varepsilon D/\delta = \mathcal{O}(1)$). The first solution, $c = 0$, corresponds to the stationary waves of Section 2, while the second solution, $u = \gamma$, yields

$$c = \pm c_c(\gamma) = \pm \frac{2}{\gamma} \sqrt{\frac{9}{\gamma^2} - 1}. \quad (6.2)$$

At $\gamma = 3$ the traveling waves collide in a pitchfork bifurcation. Below we will show that the slowly modulated traveling waves also disappear in this pitchfork bifurcation.

The construction of the slowly modulated waves closely follows that of the previous subsections.

The points $(u_{\pm}, p_R(u_{\pm}))$ at which ℓ^S and T_d intersect are given by:

$$u_{\pm} = \frac{1}{c} \left[-\tilde{\lambda}_{-} \pm \sqrt{\tilde{\lambda}_{-}^2 - 6c} \right], \quad (6.3)$$

where the condition $\tilde{\lambda}_{-}^2 - 6c \geq 0$ again gives an upper bound c_{\max} on c (ℓ^S and T_d are tangent at $c = c_{\max}$). Again, only the lower intersection point $(u_{-}, p_L(u_{-}))$ can be the basis of the construction of the modulated wave. This point determines the touch down point of an orbit that takes off at the point $(u_{-}, p_L(u_{-}))$, where, by (5.11)

$$p_L(u_{-}) = \frac{1}{2}\varepsilon(cu_{-} - \frac{6}{u_{-}}) = -\varepsilon\sqrt{\tilde{\lambda}_{-}^2 - 6c}$$

The final segment of the singular solution we need is the left slow orbit segment on \mathcal{M} given by the solution of (4.7) in the case that $\varepsilon D/\delta = \gamma$. Its general solution, in this case, is given by:

$$\begin{pmatrix} u(\xi) \\ p(\xi) \end{pmatrix} = \mathcal{A}e^{\varepsilon\delta\tilde{\lambda}_{+}\xi} \begin{pmatrix} 1 \\ \delta\tilde{\lambda}_{+} \end{pmatrix} + \mathcal{B}e^{\varepsilon\delta\tilde{\lambda}_{-}\xi} \begin{pmatrix} 1 \\ \delta\tilde{\lambda}_{-} \end{pmatrix} + \begin{pmatrix} \varepsilon/\delta \\ 0 \end{pmatrix}. \quad (6.4)$$

Imposing the initial condition $(u(0), p(0)) = (u_{-}, p_L(u_{-}))$ yields, to leading order:

$$\mathcal{A} = \frac{\varepsilon}{\delta} \left(\frac{\tilde{\lambda}_{-} - \sqrt{\tilde{\lambda}_{-}^2 - 6c}}{\tilde{\lambda}_{+} - \tilde{\lambda}_{-}} \right), \quad \mathcal{B} = -\frac{\varepsilon}{\delta} \left(\frac{\tilde{\lambda}_{+} - \sqrt{\tilde{\lambda}_{-}^2 - 6c}}{\tilde{\lambda}_{+} - \tilde{\lambda}_{-}} \right). \quad (6.5)$$

We proceed by determining the ‘time’ $\xi = \xi_{\max}$ at which we have $p(\xi) = 0$ (the Neumann boundary condition on the full solution at $x = 0$, see Figures 1 and 6). This yields:

$$\xi_{\max} = \frac{-1}{2\varepsilon\delta\sqrt{1 + \frac{1}{4}\gamma^2 c^2}} \ln \left[\frac{\tilde{\lambda}_{-}(\tilde{\lambda}_{+} - \sqrt{\tilde{\lambda}_{-}^2 - 6c})}{\tilde{\lambda}_{+}(\tilde{\lambda}_{-} - \sqrt{\tilde{\lambda}_{-}^2 - 6c})} \right], \quad (6.6)$$

and one readily verifies that when $\gamma \rightarrow 0$ this reduces to the value of $\hat{\xi}_{\max}$ calculated in (4.31) of subsection 5.3 (where $\gamma \ll 1$). However, in this more general case, we need to impose an extra condition on c , since it is not a priori clear that ξ_{\max} exists. In other words, the condition on c follows from the geometrical observation that the slow segment on \mathcal{M} through $(u_{-}, p_L(u_{-}))$ only intersects the $\{p = 0\}$ -axis when $(u_{-}, p_L(u_{-}))$ lies between ℓ^U and ℓ^S (see Figure 6). From (4.12) and (6.6) we see that only one term in the natural log expression can change sign. Thus, the existence of ξ_{\max} is equivalent to

$$\tilde{\lambda}_{+} - \sqrt{\tilde{\lambda}_{-}^2 - 6c} \geq 0,$$

or, with (6.2):

$$-c_c(\gamma) \leq c(t) \leq c_c(\gamma). \quad (6.7)$$

As a consequence, there are no slowly modulated traveling waves for $\gamma \geq 3$, ($\varepsilon D/\delta \geq 3$). In Figure 3, the line labeled \mathcal{C}_{TW} marks the bifurcation in which these traveling waves are created. It is given by $\beta = (\alpha/3) + (1/3)$, where we recall that for the purposes of Figure 3, $A = D^{\alpha}$ and $B = D^{\beta}$.

Assuming that (6.7) holds we obtain the desired integral equation for $c(t)$ by equating the above expression for ξ_{\max} with that of the distance traveled by the pulse (given in (5.18)):

$$\left[\ln \left[\frac{\tilde{\lambda}_{+} \left(\tilde{\lambda}_{+} - \sqrt{\tilde{\lambda}_{-}^2 - 6\hat{c}} \right)}{\tilde{\lambda}_{+} \left(\tilde{\lambda}_{-} - \sqrt{\tilde{\lambda}_{-}^2 - 6\hat{c}} \right)} \right] \right] = \frac{-2}{\gamma} \varepsilon^4 \delta^2 \sqrt{1 + \frac{1}{4}\gamma^2 \hat{c}^2} \int_0^t \hat{c}(s) ds, \quad (6.8)$$

where we have reintroduced the ‘hats’ on the $c(t) = \hat{c}(t)$ for clarity. Note that $\tilde{\lambda}_\pm = \tilde{\lambda}_\pm(\hat{c}(t))$ (4.12): it is possible to rewrite this equation into a differential equation for $\hat{c}(t)$ (by differentiation, as in subsection 5.4), but in this case the expression will be so complicated that it becomes prohibitive to gain additional insight in the behavior of \hat{c} as function of t .

Instead, we confine ourselves to answering two standard questions for autonomous first order ODEs: what are the critical points? and since the stable critical points are the only possible attractors, which are stable? Since the right hand side of (6.8) becomes unbounded as $\hat{c}(t) \rightarrow \hat{c}_0$, a constant, it follows that the critical points are given by $\tilde{\lambda}_+ - \sqrt{\tilde{\lambda}_+^2 - 6c} = 0$. Thus, once again, $\hat{c}_0 = 0, \pm c_c(\gamma)$. Inserting $\hat{c} = \tilde{c} \ll 1$ in (6.8) yields the ‘linearization’

$$\ln \left[\frac{1}{2}(3 - \gamma)\tilde{c} \right] = -2\varepsilon^4 \delta^2 \int_0^t \tilde{c}(s) ds.$$

Thus, by differentiation, $\hat{c}_0 = 0$ is stable, and it follows that as long as the slowly modulated waves exist (*i.e.* $\gamma < 3$), they will evolve towards the stationary wave as $t \rightarrow \infty$. Moreover, the other two critical points, $\hat{c}_0 = \pm c_c$, are unstable.

Remark 6.1. The modulated two-pulse solutions constructed here for Case **Ib** can also be found using the perturbation analysis of Section 3. Recall that in Case **Ib**, $B^{3/2}\sqrt{D/A} = \delta/\varepsilon \ll 1$ and $c^2(t) = \mathcal{O}(A)$ (*i.e.* by (4.2) and (4.5) $\gamma = \sqrt{AD}/B^{3/2} = \mathcal{O}(1)$). Hence, one needs the full formulae (3.8), (3.23) and (3.28) for μ_\pm , $(\partial/\partial\hat{\xi})(u/u_0)_{\hat{\xi}=0}$, and $(u_0)_-$, respectively, where $(u_0)_-$ is still small. Using these in (3.25), one derives an un insightful implicit relation for the slowly-varying wave speed $c(t)$. In taking $\lim_{t \rightarrow \infty} c(t) = c$, and hence also $\Gamma \rightarrow \infty$, one finds nonzero, asymptotically constant wave speeds. In particular, formula (3.23) yields: $(\partial/\partial\hat{\xi})(u/u_0)_{\hat{\xi}=0} = (3BD/u_0^2)(c/\sqrt{c^2 + 4A})$. Taking the same limit in (3.28) yields: $(u_0)_- \sim 6B^{3/2}\sqrt{(D/c^2 + 4A)}$. Hence, by (3.25), one gets the leading order relation $c = (c\sqrt{D}/6B^{3/2})\sqrt{c^2 + 4A}$. Therefore, either $c = 0$ or $c = \pm 2\sqrt{A}\sqrt{\frac{9B^3}{AD} - 1}$, to leading order, as long as $\gamma\sqrt{AD}/B^{3/2}$ is strictly $\mathcal{O}(1)$ and < 3 . The zero solution is the stationary one-pulse (Section 2), and the nonzero solutions correspond to left and right traveling waves.

Remark 6.2. Note that the existence result for traveling waves for $\varepsilon D/\delta = \mathcal{O}(1)$, or by (4.5) $AD = \mathcal{O}(B^3)$, does not contradict the non-existence result for traveling waves in [2]: there A , B and D are scaled such that $AD \ll B^3$, see Remark 2.2. We refer to [19] for the construction of different types of traveling waves.

6.2 Case IIa: Slowly-modulated two pulse solutions when $\delta/\varepsilon = \mathcal{O}(1)$

In this subsection, we establish the existence of a pair of slowly-modulated two pulse solutions in Case **IIa**, *i.e.*, when $\delta/\varepsilon = \mathcal{O}(1)$ and $\varepsilon D/\delta \ll 1$. We employ the same method as used in Section 5 and in subsection 6.1, stating only the essential steps. As in the previous section we will find that the modulated two-pulse solutions only exist up to a critical value. We define a new, $\mathcal{O}(1)$ parameter σ by $\delta = \sigma\varepsilon$ and find that the modulated pulse solutions can only exist up to $\sigma = 1/12$. At this critical value the pulse solutions merge in a homoclinic saddle node bifurcation. Geometrically this means that, in \mathcal{M} , ℓ^S and T_d are tangent at this value of σ (with $c = 0$); $\ell^S \cap T_d = \emptyset$ when $\sigma > 1/12$ so that there can neither be slowly modulated nor stationary pulse solutions for $\sigma > 1/12$. See the curve labeled \mathcal{C}_{SN} in Figure 3, which is determined by $\beta = (\alpha/3) - (1/3)$, since $\delta/\varepsilon = \mathcal{O}(1)$ here,

and we recall that we set $A = D^\alpha$ and $B = D^\beta$ for the purposes of Figure 3. This saddle node bifurcation has already been studied for the stationary pulses in subsection 4.3 of [2].

On the slow manifold \mathcal{M} , the saddle fixed point is now at $(u = 1/\sigma, p = 0)$, and its restricted unstable and stable manifolds are given by:

$$\ell^{U,S} : \quad p = \mp \varepsilon [1 - \sigma u] + \text{h.o.t.} \quad (6.9)$$

Therefore, the term linear in u is also of leading order, whereas it was of higher order in Cases **Ia** and **Ib**. Next, the zero set of ΔK is given by the line (5.7) here, just as it was in subsection 5.2, the jump in p during the fast field is also determined by (5.8), and finally the take off and touch down curves are given by (5.11) in this case, as well, all to leading order.

Due to the difference in the position of the line ℓ^S between this case and those encountered in Cases **Ia** and **Ib**, the points $(u_\pm, p_R(u_\pm))$ on \mathcal{M} at which ℓ^S intersects T_d are located at different points from that (4.25) given in subsection 5.3:

$$u_\pm = \frac{1 \pm \sqrt{1 - 6c - 12\sigma}}{c + 2\sigma}. \quad (6.10)$$

Hence, (6.10) reveals that, in order for the intersection points to exist, it must be that:

$$1 - 6c - 12\sigma > 0. \quad (6.11)$$

Otherwise, ℓ^S and T_d are tangent when $1 - 6c - 12\sigma = 0$, and there are no intersection points when this expression is negative. Moreover, (6.10) identifies the maximum wave speed $c(t)$ as:

$$c_{\max} = \frac{1}{6} - 2\sigma, \quad (6.12)$$

and, consequently, the interval $0 < \sigma < 1/12$ corresponds to the interval in which the slowly-modulated two pulse solutions exist with positive wave speed. Finally, the lower intersection point $(u_-, p_L(u_-))$ exhibits the following asymptotics:

$$u_- \rightarrow \begin{cases} \frac{1 - \sqrt{1 - 12\sigma}}{2\sigma} & \text{as } c \rightarrow 0^+, \\ 6 & \text{as } c \rightarrow c_{\max}. \end{cases} \quad (6.13)$$

Having obtained the necessary information about the lower intersection point, we now proceed to piece together the right slow, fast, and left slow segments of the instantaneous (frozen $c(t)$) pulse solution on the domain $x \geq 0$, following the same steps as in subsection 5.3. Inserting the above formula (6.10) for u_- into the equation (4.14) for the line ℓ^S yields:

$$p_R(u_-) = \varepsilon(1 - \sigma u_-) = \varepsilon \left[1 - \sigma \left(\frac{1 - \tilde{H}}{c + 2\sigma} \right) \right],$$

where we define $\tilde{H} \equiv \sqrt{1 - 6c - 12\sigma}$ in analogy with the expression H in subsection 5.3. For simplifying the further computations, we note that $c + 2\sigma = (1 - \tilde{H}^2)/6$. Next, we identify the alpha-limit set of the reduced fast homoclinic pulse, which is the point $(u_-, p_L(u_-))$ on T_o , where

$$p_L(u_-) = p_R(u_-) - \Delta p(u_-) = -\varepsilon \left(\tilde{H} + \frac{6\sigma}{1 + \tilde{H}} \right), \quad (6.14)$$

since $\Delta p(u_-) = 6\varepsilon/u_-$. This point on the take off curve lies on a hyperbolic cosine solution on \mathcal{M} inside the triangle formed by S , ℓ^U , ℓ^S and the p -axis. The explicit form of the solution is

$$u(\hat{\xi}) = \frac{1}{\sigma} + \mathcal{A}e^{\varepsilon^2\sigma\hat{\xi}} + \mathcal{B}e^{-\varepsilon^2\sigma\hat{\xi}}.$$

Imposing $(u(\hat{\xi} = 0), p(\hat{\xi} = 0)) = (u_-, p_L(u_-))$, as before, we find to leading order:

$$\mathcal{A} + \mathcal{B} = \frac{-1}{\sigma} + \frac{6}{1 + \tilde{H}} \quad \text{and} \quad \mathcal{A} - \mathcal{B} = -\left(\frac{\tilde{H}}{\sigma} + \frac{6}{1 + \tilde{H}}\right).$$

Therefore, to leading order the slow solution is:

$$\begin{aligned} u(\hat{\xi}) &= \frac{1}{2\sigma} \left[2 - (1 + \tilde{H})e^{\varepsilon^2\sigma\hat{\xi}} + \left(\tilde{H} - 1 + \frac{12\sigma}{1 + \tilde{H}} \right) e^{-\varepsilon^2\sigma\hat{\xi}} \right] \\ p(\hat{\xi}) &= \frac{-\varepsilon}{2} \left[(1 + \tilde{H})e^{\varepsilon^2\sigma\hat{\xi}} + \left(\tilde{H} - 1 + \frac{12\sigma}{1 + \tilde{H}} \right) e^{-\varepsilon^2\sigma\hat{\xi}} \right]. \end{aligned} \quad (6.15)$$

Hence, the desired time of flight along the slow manifold \mathcal{M} for the slow segment to reach the u -axis, where $p = 0$ and u is a maximum, is given explicitly by:

$$\hat{\xi}_{\max} = \frac{1}{2\varepsilon^2\sigma} \ln \left(\frac{1 - \tilde{H}}{1 + \tilde{H}} - \frac{12\sigma}{(1 + \tilde{H})^2} \right). \quad (6.16)$$

The second expression for this same time of flight comes, just as in subsection 5.5, from recalling the initial setup of the traveling wave variable: $\xi = x - \int_0^t c(s) ds$ and the subsequently-introduced scalings, so that at $x = 0$, we have

$$\hat{\xi}_{\max} = \frac{-\varepsilon^4\sigma^2}{D} \int_0^t \hat{c}(s) ds. \quad (6.17)$$

Therefore, upon equating these two expressions (6.16) and (6.17) for $\hat{\xi}_{\max}$, we have the desired (implicit) equation that determines $\hat{c}(t)$:

$$\ln \left(\frac{1 - \tilde{H}^2 - 12\sigma}{(1 + \tilde{H})^2} \right) = \frac{-2\varepsilon^6\sigma^3}{D} \int_0^t \hat{c}(s) ds. \quad (6.18)$$

Differentiating both sides of (6.18) with respect to t (and doing a little algebra) yields:

$$\frac{d\hat{c}}{dt} = \frac{-2\varepsilon^6\sigma^3}{D} \hat{c}^2 \sqrt{1 - 6\hat{c} - 12\sigma} \left(\frac{c + 2\sigma}{c + 2\sigma\sqrt{1 - 6\hat{c} - 12\sigma}} \right). \quad (6.19)$$

We conclude that the additional terms in (6.19) compared to (5.20) do not influence the qualitative behavior of $\hat{c}(t)$: there is an upper bound on \hat{c} that is approached as t becomes small and $\hat{c} \rightarrow 0$ monotonically (as $1/t$) when $t \rightarrow \infty$. Moreover, one can recover (5.20) from (6.19) by replacing σ with δ/ε in (6.19) and taking the limit $\delta/\varepsilon \ll 1$.

Remark 6.3. As mentioned, in Case **IIa**, unlike in cases **Ia** or **Ib**, the second point $(u_+, p_R(u_+))$ at which ℓ^S and T_d intersect can also give rise to two-pulse orbits. We restrict attention to the triangle in the first quadrant of the $c - \sigma$ plane bounded above by $c = -2\sigma + (1/6)$. From

(6.10) and the definition of \tilde{H} , $u_+ = 6/(1 - \tilde{H})$, one finds: $p_R(u_+) = \varepsilon[1 - (6\sigma/1 - \tilde{H})]$ and also $p_L(u_+) = p_R(u_+) - (6\varepsilon/u_+) = \varepsilon[\tilde{H} - (6\sigma/1 - \tilde{H})]$. Clearly, there is now a possibility to have $p_L < 0$. This condition is equivalent to $6(c + \sigma)^2 - c > 0$. Then, by direct calculation, one verifies that there is a subset of the triangle in which this condition holds, namely it holds for all (c, σ) pairs with $1/24 \leq \sigma < 1/12$, and when $0 < \sigma < 1/24$ it holds for those (c, σ) pairs in which either $c > c_+$ or $c < c_-$, where $c_{\pm}(\sigma) = (1/12) - \sigma \pm (1/12)\sqrt{1 - 24\sigma}$.

7 Stability analysis for slowly-modulated two pulse solutions

In this section, we carry out a formal linear stability analysis for the slowly-modulated two pulse solutions constructed in the previous sections. In particular, we determine whether or not there exist directions along which infinitesimal perturbations of the quasi-stationary two-pulse solutions grow exponentially. Of course, the use of the quasi-stationary approximation imposes a restriction on the instabilities one can detect with the approach used here, namely we can only check for disturbances that grow on a time scale that is shorter than that corresponding to the rate of change of U_t , V_t , and the rate of change of the wave speed in time (see subsection 5.6). We follow the ideas developed in [3] for the stability analysis of the stationary 1-pulse patterns of (1.1) which was done there in the special scaling of [2] (see Remark 2.2). We refer to [3] for some of the technical and computational details of the ‘NLEP method’. The validity of this method has been established by a stability index analysis in [4], and it has been shown in [5] that this method can be applied to a large class of reaction-diffusion equations.

This section is organized as follows. In subsection 7.1, we state the scaled fourth-order eigenvalue problem. In subsection 7.2, we treat Case **I** by reducing the full problem to a second-order nonlocal eigenvalue problem and analyzing this reduced system. Cases **IIa** is discussed in subsection 7.3; the details of the analysis are given in Appendix B.

7.1 The scaled fourth-order eigenvalue problem

The Gray-Scott model (1.1) written in the unscaled modulated traveling wave variable is:

$$U_t = U_{\xi\xi} + c(t)U_{\xi} - UV^2 + A(1 - U), \quad V_t = DV_{\xi\xi} + c(t)V_{\xi} + UV^2 - BV. \quad (7.1)$$

Let $(u_0(\xi), v_0(\xi))$, denote a quasi-stationary, slowly-modulated two pulse solution, where the $c(t)$ dependence is implicit. Stability with respect to small perturbations is determined by setting

$$U(\xi, t) = u_0(\xi) + u(\xi)e^{\lambda t} \quad \text{and} \quad V(\xi, t) = v_0(\xi) + v(\xi)e^{\lambda t}, \quad (7.2)$$

and then by studying the linearized eigenvalue problem:

$$\lambda u = u_{\xi\xi} + cu_{\xi} - v_0^2 u - 2u_0 v_0 v - Au, \quad \lambda v = Dv_{\xi\xi} + cv_{\xi} + v_0^2 u + 2u_0 v_0 v - Bv. \quad (7.3)$$

As was shown in [3] for the stability of the stationary solutions (namely in the $c = 0$ case of (7.3)), the significant scaling of the variables (and here also of the wave speed) in this eigenvalue problem is the same as that used in the existence analysis. Recalling (4.2), let:

$$\xi = \sqrt{\frac{D}{B}}\hat{\xi}, \quad u(\xi) = B^{3/2}\sqrt{\frac{D}{A}}\hat{u}(\hat{\xi}), \quad v(\xi) = \sqrt{\frac{A}{BD}}\hat{v}(\hat{\xi}), \quad c = \frac{A\sqrt{D}}{B^{3/2}}\hat{c}, \quad (7.4)$$

and scale u_0 and v_0 as in (4.2), so the eigenvalue problem (7.3) becomes:

$$\begin{aligned}\hat{u}_{\hat{\xi}\hat{\xi}} &= \frac{A}{B^2} \left[(\hat{v}_0^2 \hat{u} + 2\hat{u}_0 \hat{v}_0 \hat{v}) + BD \left(1 + \frac{1}{A} \lambda \right) \hat{u} - D \hat{c} \hat{u}_{\hat{\xi}} \right] \\ \hat{v}_{\hat{\xi}\hat{\xi}} + \left[2\hat{u}_0 \hat{v}_0 - \left(1 + \frac{\lambda}{B} \right) \right] \hat{v} &= -\hat{v}_0^2 \hat{u} - \frac{A}{B^2} \hat{c} \hat{v}_{\hat{\xi}}.\end{aligned}\tag{7.5}$$

Finally, we scale the eigenvalue parameter as

$$\lambda = B \hat{\lambda},\tag{7.6}$$

see the Appendix of [3], and, in the stability analysis, we again use: $\varepsilon = \sqrt{A}/B \ll 1$ and $\delta = \sqrt{BD} \ll 1$ (4.5) with $\delta/\varepsilon \leq \mathcal{O}(1)$. Therefore, dropping hats, we arrive at the final form of the eigenvalue problem to be studied in this section:

$$\begin{aligned}u_{\xi\xi} &= \varepsilon^2 (v_0^2 u + 2u_0 v_0 v) + \varepsilon^2 \delta^2 u + D \lambda u - \varepsilon^2 D c u_{\xi} \\ v_{\xi\xi} + [2u_0 v_0 - (1 + \lambda)] v &= -v_0^2 u - \varepsilon^2 c v_{\xi}.\end{aligned}\tag{7.7}$$

7.2 Transformation of the eigenvalue problem to a second-order NLEP

In this subsection, we reduce the full fourth-order eigenvalue problem (7.7) to a second-order nonlocal eigenvalue problem (NLEP). We treat Case **Ia** in detail in this subsection and discuss Case **IIa** in subsection 7.3 (and Appendix B). This analysis extends to the $c(t) > 0$ case the procedure for deriving an NLEP previously introduced in [3] for the $c = 0$ case. In this section we will assume that $D \ll 1$; as a consequence we will find that the first derivative terms with factors of $c(t)$ in them are of higher order. This simplifies the analysis considerably. The case $D \geq \mathcal{O}(1)$ is discussed in Remark 7.2.

The essence of the procedure for deriving the NLEP is to exploit the fast-slow structure of the underlying quasi-stationary solution to determine the fast-slow structure of the eigenfunctions. In particular, we recall that $v_0(\xi)$ is exponentially small in the slow regimes. Hence, the first equation in (7.7) reduces to:

$$u_{\xi\xi} = \varepsilon^2 \delta^2 u + D \lambda u - \varepsilon^2 D c u_{\xi} + \text{expo, small}.\tag{7.8}$$

Therefore, the u component of the eigenfunction consists of slow segments along which u undergoes slow exponential decay as $|x| \rightarrow \infty$, and there is also a jump discontinuity in u_{ξ} across $\xi = 0$, since there is a difference between the slopes of the right and left slow solutions as $|\xi|$ approaches zero. We label this jump discontinuity in the slow field (expressed in the scaled variables) by $\Delta_s u_{\xi}$, and it plays an essential role, as we saw in [3].

To determine the leading order behavior of $\Delta_s u_{\xi}$, we analyze the terms in the slow u equation (7.8). The third term on the right is always subdominant to the second, because $\varepsilon \ll 1$. The dominant term is then either the second or the first term, or both, depending on whether one is in:

$$\text{Regime 1 : } \varepsilon^2 \delta^2 \ll D, \quad \text{Regime 2 : } \varepsilon^2 \delta^2 \gg D, \quad \text{or} \quad \text{Regime 3 : } \frac{\varepsilon^2 \delta^2}{D} = \mathcal{O}(1),$$

Remark 7.1. It must be noted that $\varepsilon^2 \delta^2 = AD/B$. In other words these three regimes are more simply defined by: Regime 1: $A \ll B$; Regime 2: $A \gg B$; and, Regime 3: $A/B = \mathcal{O}(1)$.

Next, we recall that the fast regime is a narrow interval about $\xi = 0$ and, in this interval, $v_0(\xi)$ possesses a pulse. Hence, to leading order in the fast regime $u_{\xi\xi} = \varepsilon^2(v_0^2 u + 2u_0 v_0 v) + D\lambda u$, which implies that the u component of the eigenfunction is constant to leading order for $\varepsilon \ll 1$ and for small D . We label this constant κ . Moreover, the derivative u_ξ has a jump discontinuity:

$$\Delta_f u_\xi = \varepsilon^2 \int_{-\infty}^{\infty} (u v_0^2 + 2u_0 v_0 v) d\xi + D\lambda \int_{-\infty}^{\infty} u d\xi + \text{h.o.t.} \quad (7.9)$$

Here, we note that the limits have been obtained from the appropriate (exact) ε - and δ -dependent times at which the pulse enters and exits the fast field and then sending ε and $\delta \rightarrow 0$. Hence, the integral of the constant has a finite value (see [3, 4]).

Finally, the transformation to the NLEP is completed by determining the constant κ . This is now done on a regime-by-regime basis for different regimes in the $\varepsilon - \delta - D$ parameter space. We will match the jump discontinuities $\Delta_s u_x$ and $\Delta_f u_\xi$, as computed in the slow and fast fields, respectively, and obtain formulae for κ . Different terms will be of leading order in different regimes.

Remark 7.2. The stability of the stationary 1-pulse patterns (see Section 2) follows immediately from the results in this section by setting $c \equiv 0$. As a consequence, we do not have to assume that $D \ll 1$ when studying these 1-pulse patterns. The case $D \geq \mathcal{O}(1)$ is a subcase of Regime 1. We will find in subsection 7.2.1 that the pulse patterns are always unstable for $\varepsilon^2 \ll \sqrt{D}$, i.e. there cannot be stable pulse solutions when $D \geq \mathcal{O}(1)$ (in the parameter regime studied in this paper, see remark 1.1). By construction, the modulated two-pulse solutions evolve toward 2 copies of these stationary 1-pulse solutions as $t \rightarrow \infty$. Therefore, it is only of limited relevance to consider the case $D \geq \mathcal{O}(1)$ for the modulated two-pulse patterns, since these solutions cannot be stable (at least not for t large), see also subsection 5.6.

7.2.1 Regime 1

In this subsection, we treat Regime 1 in detail. Since $\varepsilon^2 \delta^2 \ll D$, equation (7.8) implies that the left and right slow segments of u are given (in terms of the fast variable) to leading order by:

$$u(\xi) = \kappa e^{\pm\sqrt{D}\lambda\xi}. \quad (7.10)$$

Hence, between the left and right slow solutions, the jump discontinuity in u_ξ is to leading order:

$$\Delta_s u_\xi = \lim_{\xi \rightarrow 0^-} u_\xi - \lim_{\xi \rightarrow 0^+} u_\xi = -2\sqrt{D}\lambda\kappa. \quad (7.11)$$

In order to match this slow jump discontinuity to the fast jump discontinuity $\Delta_f u_\xi$ given by (7.9), we first assume $\varepsilon^2 \gg D$, so that the first term in the right hand side of (7.9) is the dominant term. This is done largely to facilitate the analysis, and the complementary regime ($\varepsilon^2/D \leq \mathcal{O}(1)$) will be treated separately at the end of this subsection. The explicit leading order matching condition needed to determine κ is then readily at hand:

$$-2\sqrt{D}\lambda\kappa = \varepsilon^2 \left[\kappa \int_{-\infty}^{\infty} v_0^2 d\xi + 2u_0 \int_{-\infty}^{\infty} v_0 v d\xi \right]. \quad (7.12)$$

Since the scaling included the assumption $\lambda = \mathcal{O}(1)$, there are three subregimes to consider:

$$\mathbf{1a} : \varepsilon^2 \ll \sqrt{D}, \quad \mathbf{1b} : \varepsilon^2 = \mathcal{O}(\sqrt{D}), \quad \mathbf{1c} : \varepsilon^2 \gg \sqrt{D}. \quad (7.13)$$

In subregime **1a**, the matching condition (7.12) directly yields $\kappa = \mathcal{O}(\varepsilon^2/\sqrt{D}) \ll 1$, *i.e.* the constant value of u to leading order during the fast jump is asymptotically small. Hence, the coupling of the slow field to the fast field is weak (*i.e.*, of higher order), and the leading order fast eigenvalue problem is precisely that associated to a single isolated fast homoclinic pulse:

$$v_{\xi\xi} + [2u_0v_0 - (1 + \lambda)]v = 0,$$

which has a (scaled) positive eigenvalue at $\lambda = 5/4$. Therefore, since the higher order terms will only displace this eigenvalue by a small amount, there exists an eigendirection along which small perturbations of the slowly-modulated two-pulse solution lead to exponential growth, and one may say that these solutions are formally unstable in subregime **1a**.

In subregime **1b**, where $\varepsilon^2 = \mathcal{O}(\sqrt{D})$, we introduce the new $\mathcal{O}(1)$ parameter

$$d = \frac{\sqrt{D}}{\varepsilon^2}, \tag{7.14}$$

and remark that $d = \sqrt{D}B^2/A$ in the original parameters. All of the terms in the leading order matching condition (7.12) are now retained, and one finds:

$$\kappa = \frac{-u_0^3}{3 + d\sqrt{\lambda}u_0^2} \int_{-\infty}^{\infty} v_0(\xi)v(\xi)d\xi, \tag{7.15}$$

Here we have again used $\int_{-\infty}^{\infty} v_0^2(\xi)d\xi = 6/u_0^2$. Clearly, this value of κ is of $\mathcal{O}(1)$, since d , u_0 , and λ are $\mathcal{O}(1)$. Hence, by replacing the variable u with its leading order constant value κ over the fast field on the right hand side of the second equation in (7.7), by neglecting the higher order cv_ξ term, and by recalling κ from (7.15), we find that the leading order eigenvalue problem becomes:

$$v_{\xi\xi} + [2u_0v_0 - (1 + \lambda)]v = -\kappa v_0^2. \tag{7.16}$$

This turns out to be exactly the same NLEP analyzed in case II of subsection 5.2 in [3] ($\beta = 1/2$), that is the significant scaling in which the solutions gain stability through a Hopf bifurcation (this is not surprising since the parameters A, B, D are also related by $\varepsilon^2 = A/B^2 = \mathcal{O}(\sqrt{D})$ for $\beta = 1/2$ in [3]). To make this correspondence precise, we simplify the notation in the expression for u_- , which we recall from (5.12) is: $u_{\pm} = \frac{1}{c(t)} \left(1 \pm \sqrt{1 - 6c(t)}\right)$. We introduce a new parameter $\ell = \ell(t)$ via: $u_- = 3\ell$. This new parameter will help greatly to keep the algebra to a minimum. Explicitly,

$$\ell = \frac{1}{3c} \left(1 - \sqrt{1 - 6c}\right). \tag{7.17}$$

Hence, we know $\ell \in (1, 2)$ for all $0 < c(t) < 1/6$, since $\ell \rightarrow 1$ as $c \rightarrow 0$, $\ell \rightarrow 2$ as $c \rightarrow c_{\max} = 1/6$, and ℓ is a monotonically increasing function of c on $(0, 1/6)$. (Also, $d\ell/dc \sim 3/2$ as $c \rightarrow 0$ and $d\ell/dc \rightarrow +\infty$ as $c \rightarrow 1/6$.)

Next, we follow the procedure used in Section 5 in [3], and change the independent and dependent variables and parameters in the NLEP (7.16). Let $t = \xi/2, y(t) = v(\xi)$ and

$$P^2 = 4(1 + \lambda) \quad \text{and} \quad C = \frac{9}{1 + 3d\ell^2\sqrt{\lambda}}. \tag{7.18}$$

The NLEP (7.16) then becomes:

$$\ddot{y} + [12\text{sech}^2(t) - P^2]y = C\text{sech}^4(t) \int_{-\infty}^{\infty} y(t)\text{sech}^2(t)dt, \quad (7.19)$$

where $\dot{} = d/dt$, and we used $v_0(\xi) = (3/2u_0)\text{sech}^2(\xi/2)$ and $u_0 = u_- = 3\ell$. Inverting the formula for C we get:

$$d\ell^2(t) = \frac{2}{3\sqrt{P^2 - 4}} \left[\frac{9}{\mathcal{C}(P)} - 1 \right], \quad (7.20)$$

where $\mathcal{C}(P)$ is an explicitly known expression in terms of integrals over hypergeometric functions, see subsection 5.1 in [3] for the derivation of $\mathcal{C}(P)$. This formula should be interpreted as follows: an eigenvalue λ of (7.7) corresponds by (7.18) to a solution P of (7.20). Note that this implies that $\lambda = \lambda(t)$, *i.e.* the eigenvalues λ of the linearized stability problem (7.7) vary on the same slow time scale τ (5.25) as the speed c .

Formula (7.20) is identical to formula (5.15) from [3] with $a = \sigma = m = 1$ and $b^2 = d\ell^2(t)$. Therefore, it follows from the hypergeometric functions analysis in [3] (see (5.16) and Figure 5 in [3]) that there are no eigenvalues λ with $\text{Re}(\lambda) > 0$ when

$$d\ell^2(t) \leq d_H \approx (0.66)^2 \approx 0.44 \quad (7.21)$$

Since $\ell(t)$ decreases monotonically from 2 to 1 we can conclude that the modulated two-pulse solutions are formally stable for all t when

$$d \leq \frac{d_H}{4} \approx 0.11, \quad \text{i.e. } D < 0.012\dots\varepsilon^2 \quad \text{or} \quad DB^4 < 0.012\dots A \quad (7.22)$$

(by (7.14), (4.5)). Moreover, all modulated two pulse solutions (including the limiting stationary 1-pulse solutions) are unstable when

$$d \geq d_H \approx 0.44, \quad \text{i.e. } D > 0.19\dots\varepsilon^2 \quad \text{or} \quad DB^4 > 0.19\dots A. \quad (7.23)$$

For $0.11 < d < 0.44$, *i.e.* $0.012\varepsilon^2 < D < 0.19\varepsilon^2$, the situation is more ‘dynamic’. We know from [3] that there are no eigenvalues $\lambda(t)$ with $\text{Re}(\lambda(t)) > 0$ when $d\ell^2(t) \leq d_H$ (7.21), moreover there are 2 unstable eigenvalues when $d\ell^2(t) > d_H$. Therefore, we define for a given $d \in (d_H/4, d_H) \approx (0.11, 0.44)$ a critical value of ℓ , $1 < \ell_* < 2$ such that $d\ell_*^2 = d_H \approx 0.44$. The modulated two pulse solution is then stable for all $t > t_*$ where t_* is defined by $\ell(t_*) = \ell_*$ since both eigenvalues have crossed the imaginary axis at $t = t_*$. Equivalently, it is unstable for $t < t_*$. Note that this implies that the limiting solutions, the stationary 1-pulse solutions, are stable for all $d < d_H$. However, a pair of two pulse solutions will only be stable (*i.e.*, numerically observable) for $d \in (d_H/4, d_H)$ when the distance between the two pulses is ‘large enough’.

The bifurcation at which the 2 eigenvalues cross the imaginary axis is a Hopf bifurcation: the eigenvalues are a complex conjugate pair and purely imaginary at the bifurcation. These two eigenvalues merge and become real as d , or $d\ell^2$, is increased, see again [3] for explicit calculations. In the limit $d \gg 1$, *i.e.* in the transition from Regime **1b** to Regime **1a**, one of these eigenvalues will approach $5/4$, the other decreases towards 0. Thus, we have recovered the instability result of Regime **1a** and deduced the existence of a second unstable eigenvalue near 0 in this case. Using (7.20) we can write down an explicit approximation for this eigenvalue, using the fact that $\mathcal{C}(P) \rightarrow 9/2$ as $P \rightarrow 2$, *i.e.* $\lambda \rightarrow 0$ by (7.18), see [3]: for $d \gg 1$

$$\lambda(t) = \frac{4}{9d\ell^4(t)} \ll 1 \quad \text{or} \quad \lambda(t) = \frac{4}{9\ell^2(t)} \frac{\varepsilon^4}{D} \ll 1 \quad (7.24)$$

(at leading order). This eigenvalue will yield the instability result in the case $D \geq \varepsilon^2$ at the end of this subsection.

Next, we turn to subregime **1c**. The stability result of Regime **1b** (7.22) can be extended into this regime in a natural fashion, since $d \ll d_H/4$ in Regime **1c**. Thus, since $\sqrt{D} \ll \varepsilon^2$ we can take the limit $d \rightarrow 0$ in (7.15) and derive:

$$\kappa = \frac{-u_0^3}{3} \int_{-\infty}^{\infty} v_0(\xi)v(\xi)d\xi, \quad (7.25)$$

i.e., the left hand side of (7.12), the slow jump in u_ξ , has become of higher order compared to the right hand side, the fast jump in u_ξ . It follows from the analysis in [3] that both eigenvalues that crossed the imaginary axis in Regime **1b** remain at the stable side of this axis in this limit. In fact, with this value of κ , the NLEP (7.16) is the same as that derived in case III of subsection 5.2 in [3], namely in the regime where the parameter β there satisfies $1/2 < \beta < 1$. Hence, we may conclude directly that all of the slowly-modulated two pulse solutions are formally stable with respect to infinitesimal perturbations in this subregime.

Finally, in Regime **1**, we skipped the case $D \geq \mathcal{O}(\varepsilon^2)$, which includes the case $D \geq \mathcal{O}(1)$. Here, we do get the same instability result as in subregime **1a**. However, the instability is not caused by the unstable eigenvalue found near 5/4. This eigenvalue cannot exist when $D \gg \varepsilon^2$ since then the u -component of the eigenvalue problem (7.7) is given by $u_{\xi\xi} = D\lambda u$ at leading order, both in the fast field and in the slow field. Therefore, there are for $\lambda = \mathcal{O}(1)$ no eigenfunctions that are bounded as $|x| \rightarrow \infty$. Nevertheless, the eigenvalue of $\mathcal{O}(\varepsilon^4/D) \ll 1$ with $\lambda \ll 1$, (7.24), is still there. Its construction is not influenced by the fact that $D \gg \varepsilon^2$ since the term $D\lambda u$ is once again only of higher order (in the fast field) for a λ of this magnitude. We may conclude that the unstable eigenvalue (7.24) exists for all $D \geq \mathcal{O}(\varepsilon^2)$ and thus that the slowly-modulating two pulse solutions are also formally unstable in this part of Regime 1.

7.2.2 Regime 2

In this regime, $D \ll \varepsilon^2\delta^2$, so that the first equation (7.8) is to leading order $u_{\xi\xi} = \varepsilon^2\delta^2u$. Hence, the left and right slow segments (expressed in terms of the fast variable) are to leading order $u(\xi) = \kappa e^{\pm\varepsilon\delta\xi}$, and the leading order jump discontinuity in u_ξ at $x = 0$ between them is:

$$\Delta_s u_\xi = -2\varepsilon\delta\kappa. \quad (7.26)$$

The corresponding jump discontinuity at $x = 0$ in the fast field is given by the first term in (7.9):

$$\Delta_f u_\xi = \varepsilon^2 \int_{-\infty}^{\infty} (\kappa v_0^2 + 2u_0 v_0 v) d\xi. \quad (7.27)$$

Finally, matching these leading order jump discontinuities, *i.e.*, equating (7.26) and (7.27), and recalling $\delta/\varepsilon \ll 1$, we recover (7.25). This is not surprising since, as in Regime **1c**: $\Delta_s u_\xi \ll \Delta_f u_\xi$. Thus, like in Regime **1c**, we can immediately conclude that the slowly-modulating two pulse solutions are linearly stable in Regime 2 by referring to the analysis for Case III in subsection 5.3 of [3].

7.2.3 Regime 3

In this final regime, $\varepsilon^2 \delta^2 / D = \mathcal{O}(1)$, and we introduce the new $\mathcal{O}(1)$ parameter $s = \varepsilon^2 \delta^2 / D$. The slow eigenvalue problem (7.8) becomes to leading order $u_{\xi\xi} = D(s + \lambda)u$, and hence the relevant jump discontinuity in the slow field is

$$\Delta_s u_\xi = -2\sqrt{D(s + \lambda)}\kappa. \quad (7.28)$$

The jump in u_ξ in the fast field is still given by (7.9). Therefore, the matching condition is:

$$-2\sqrt{D(s + \lambda)}\kappa = \varepsilon^2 \int_{-\infty}^{\infty} (uv_0^2 + 2u_0v_0v) d\xi + D\lambda \int_{-\infty}^{\infty} u d\xi + \text{h.o.t.} \quad (7.29)$$

Now, there are three subregimes as we saw in Regime 1, and the analysis of these proceeds in the same fashion. In fact, the results from regime 1 may be applied directly here after taking into account the shift in the spectrum by the parameter-dependent amount s .

Remark 7.3. Although we divided the parameter space up into a number of (sub)regimes, there is only one in which there is a transition from stable to unstable, subregime **1b**, where $\varepsilon^2 = \mathcal{O}(\sqrt{D})$. This relation determines the curve $\mathcal{C}_{\text{HOPF}}$ in Figure 3.

7.3 Stability in Case IIa

In this subsection we will only give a brief sketch of the stability properties, the details are presented in Appendix B.

There are two important subregimes in saddle-node bifurcation Case **IIa**, where $\varepsilon = \mathcal{O}(\delta)$ (subsection 6.2): $\varepsilon^2 \ll \sqrt{D}$ and $\varepsilon^2 \gg \sqrt{D}$. Referring to Figure 3 we see that the line \mathcal{C}_{SN} is to the right of $\mathcal{C}_{\text{Hopf}}$ in the first regime, while \mathcal{C}_{SN} is to the left of $\mathcal{C}_{\text{Hopf}}$ in the second regime (note that both $A \gg 1$ and $B \gg 1$ here). Therefore, it is a rather straightforward extension of the analysis in the previous subsection, to show that in the first regime all pulse solutions are unstable with respect to perturbations associated to a pair of complex conjugate eigenvalues with $\text{Re}(\lambda) > 0$.

However, in the second regime, there are no complex eigenvalues, as in Regimes **1c** and **2** above. Yet, the stability analysis has become somewhat more involved, due to the more complicated structure of the pulse solutions themselves. In Appendix B we show that the modulated pulse solution constructed in subsection 6.2 are stable for $\sigma = \delta/\varepsilon$ below a certain critical value that varies slowly in time (and that can be determined explicitly). The situation here is similar to that in the transition case $d_H/4 < d < d_H$ of subregime **1b**: the pulse solutions all become stable after a certain time. The stationary 1-pulse solution is stable as long as it exists (for all $\sigma < 1/12$). The bifurcation is truly a saddle-node bifurcation, since it can be shown that the other modulating two pulse pattern and its stationary 1-pulse limit (Remark 6.3) are always unstable.

Remark 7.4. We did not consider the stability of the modulating two pulse solutions or of the traveling waves in Case **Ib**. The NLEP method can be used to studied this, although one should not underestimate the necessary computations.

8 Numerical simulations and discussion

8.1 The essential role of the slowly-varying $U(x, t)$

The existence and stability results presented in this work naturally lead to some questions and observations about various aspects of pulse splitting. We focus here on those in which the slow variation of $U(x, t)$ plays a central role.

The stability analysis of Section 7 shows that there is a large domain in the parameter space in which both the stationary 1-pulse patterns of Section 2 (and [2]) and the slowly modulated two-pulse solutions are stable, see Figure 3. Part of the boundary of this domain is given by a line $A = \mathcal{O}(B^2)$, and it is precisely when this line $\mathcal{C}_{\text{SPLIT}}$ is crossed that the one-pulse patterns no longer exist (see Section 6 of [3]) and that the self-replication process starts [3]. In particular, it can be shown that there is a critical value of ε , $\varepsilon_{\text{split}}$, so that for $\delta \ll 1$ there exists a stationary 1-pulse homoclinic solution to (1.1) for all $\varepsilon < \varepsilon_{\text{split}}$. This result was obtained in Section 6 of [3] using topological shooting arguments in the special choice for the parameters A, B, D as given in Remarks 2.2, 3.1. Since the scaled ODE (6.1) in [3] has the same essential structure as the ODE (4.6) here in so far as the topological shooting is concerned, a duplication of the arguments given in [3] shows that the stationary homoclinic one-pulse solution of (4.6) cannot exist for

$$\varepsilon > \varepsilon_{\text{split}} \quad \text{i.e.,} \quad A > \varepsilon_{\text{split}}^2 B^2.$$

In the terminology of [3], the solution ‘disappears,’ and numerically, one observes the start of the self-replication process for $\varepsilon > \varepsilon_{\text{split}}$. In addition, it was found in [24, 23, 2, 25, 3, 21, 19] that there are stable periodic multi-pulse patterns that appear as end products of the self-replicating process. These solutions were constructed in [2]: their structure in phase space is very similar to that of the homoclinic pattern: the solution is close to the slow manifold except for a homoclinic ‘jump’ through the fast field (see Figure 2 in [2]).

These observations raise two questions: why do (some of) the periodic multi-pulse patterns still exist for $\varepsilon > \varepsilon_{\text{split}}$? and, why does the pair of outward modulating pulses still exist for $\varepsilon > \varepsilon_{\text{split}}$ (as can be observed in the numerical simulations, see Figure 2)? After all, the construction of both of these types of solutions is based on the same asymptotic method that breaks down for the stationary 1-pulse at $\varepsilon = \varepsilon_{\text{split}}$.

The formal answer to both these questions can be found by examining the magnitude and dynamics of $U(x, t)$ in the region where $V(x, t)$ has a pulse. For both of these types of solutions, the value of U in the pulse intervals is *significantly larger* than that of the stationary 1-pulse. For the traveling pulses this can be seen, in terms of the scalings (4.2) $U(x, t) \approx (u_0)_- = (\delta/\varepsilon)u_-$ in a pulse interval, from (3.29) in Section 3 or from (5.12) in Section 5, as follows: whereas one finds $u_- \approx 6$ at the initial stage of the splitting process (where c is near its maximum $1/6$), one sees that $u_- = 3$ for the stationary pulse ($c = 0$). Similarly, for the multi-pulse spatially periodic patterns, formula (2.9) in [3] shows that the value of u_- is much larger than that of the stationary one-pulse.

What is the importance of this fact that the U values are significantly larger? and correspondingly that the amplitudes V are smaller (see (2.2), (3.6), (5.2))? Observe that in the (u, p) -equations of (4.6) $\ddot{u} = \varepsilon^2[uv^2 + \text{h.o.t.}]$, the term with v depends on u . As in Sections 2 and 3 (see (2.2), (3.6)), one can reexpress this u dependence (to leading order) by introducing \hat{v} : $v(\xi) = \hat{v}(\xi)/u$;

where \hat{v} is now a solution of $\ddot{\hat{v}} = -\hat{v}^2 + \hat{v}$, that is independent of u to leading order (see also (3.16)). Hence, the leading order equation is:

$$\ddot{u} = \frac{\varepsilon^2}{u}[\hat{v}^2 + \text{h.o.t.}],$$

and the leading order influence of u occurs through the factor ε^2/u , which may be labeled as an ‘effective’ value of ε . This implies that those solutions having a higher value of u during the pulse interval are really solutions of a system that has a lower effective ε . Interpreting this for modulating two-pulse solutions, we see that they can exist in the regime where the actual ε is greater than $\varepsilon_{\text{split}}$ as long as the value of U is large enough so that the effective ε lies below $\varepsilon_{\text{split}}$. In this way, this solution can exist in a regime where the stationary one-pulse no longer does. A similar argument can be made for the multi-pulse solutions. This explains heuristically the existence of both the pairs of traveling pulse solutions and the singular periodic multi-pulse solutions, respectively, in the regime $\varepsilon > \varepsilon_{\text{split}}$, where the stationary one-pulse no longer exists.

The same heuristic extrapolations of the asymptotic analysis explain why two slowly-modulating pulses traveling apart from each other split again after long enough time (on a large enough interval). Once again the value of U on intervals in which V has a pulse is the key to understanding this: $c(t)$ decreases monotonically to 0, and therefore, by (5.12), u_- decreases slowly from 6 to 3, the value of the stationary pulse. Thus, the ‘effective ε ’ has increased to above $\varepsilon_{\text{split}}$. Moreover, for the modulating two-pulses this also yields a certain time T_{split} corresponding to when the effective value of ε crosses through $\varepsilon_{\text{split}}$ (*i.e.*, the value of u_- becomes small enough), and both traveling pulses undergo splitting. The time T_{split} will depend on $\Delta\varepsilon = \varepsilon - \varepsilon_{\text{split}}$, and T_{split} decreases as $\Delta\varepsilon$ increases, as can be checked by numerical simulations. However, it should be noted that simulations of this mechanism are highly sensitive to boundary effects, and one must be sure to work on a sufficiently large domain (see subsection 8.3).

The above arguments are far from rigorous. The most important obstacle is the fact that $\varepsilon_{\text{split}}$ is not an asymptotically small value. On the contrary, it is a well-defined $\mathcal{O}(1)$ number, see Table 1 in [3]. Thus, we cannot expect that ‘ u is constant to leading order’ or that ‘ \hat{v} does not depend on u to leading order’ in ‘*the fast field*’: this terminology is only applicable when ε is asymptotically small and one can do a perturbation analysis. Nevertheless, the existence of an $\varepsilon_{\text{split}}$ value for slowly-modulating two-pulse solutions can be made rigorous by employing the same topological shooting method as was established in [3] for the stationary one-pulse solutions. We do not consider this in any more detail in this paper.

In addition, we did not pay any attention to the ‘leading order’ perturbations of $\mathcal{O}(\varepsilon^2)$ in the \hat{v} -equation, although one can argue on formal grounds that these ‘perturbations’ do not give a net contribution.

On a bounded interval, the splitting process will come to a halt as soon as the outward traveling pulses approach the boundary of the domain [24, 23, 2, 25, 3, 21, 19]. The solution will settle in a periodic multi-pulse pattern that has a ‘large enough’ value of U in the V -pulses. It has been checked in [3] that this multi-pulse pattern will also split as soon as ε is increased above a certain critical value, which depends monotonically on the wave length, *i.e.* the distance between the pulses of the pattern. See Table 3 in [3]. This is consistent with the heuristic arguments: the effective value of ε also increases when ε increases.

Finally, the reduction of the effective value of ε cannot be larger than $\mathcal{O}(1) \times \varepsilon$. Therefore,

one cannot expect to see the traveling pulses for ε ‘far’ from $\varepsilon_{\text{split}}$, *i.e.* for $\Delta\varepsilon$ ‘too large.’ At first, it seems that this contradicts the numerical simulations in [24, 23, 2, 25, 21, 19]; however, a more careful study of these simulations reveals that there is no contradiction. On the contrary, these simulations are consistent with our arguments, since they indicate that the traveling pulses are no longer of the type studied in this paper when $\Delta\varepsilon$ becomes ‘too large.’ Numerous figures in [24, 23, 2, 25, 21, 19] clearly show that, in this case, the speed c of the (most) outward traveling pulses *does not decrease* as a function of time between two successive splittings. Furthermore, these pulses are *not stationary* in a coordinate system traveling with speed c : the shape of the pulses changes as function of time, especially at the trailing edges of the pulses, see Figure 7 here, Figure 9 in [2], or Figure 5.3 in [21]. Thus, these pulses are of an essentially different type. These simulations also strongly suggest that these traveling pulses can even be stable for certain parameter combinations: Figure 5.3 in [21] shows a solitary pulse traveling with constant speed with a periodic modulation of its trailing edge. Moreover, the distinction between a splitting process with pulses whose speeds slowly decrease to 0 for ε near $\varepsilon_{\text{split}}$ and a splitting process with pulses whose speeds are constant for ε not near $\varepsilon_{\text{split}}$ is of course not exact: numerical simulations also show that there is a transition region where the speed of the pulses first decreases slowly, but after some time (on the slow time scale), the speed remains constant, > 0 . The existence analysis for these intriguing constant speed solutions asks for an approach that differs essentially from that in this paper, since these solutions appear from numerical simulations to exist only in regions where the existing asymptotic methods are not applicable. On the other hand, some perturbation analysis may be possible, since the shape of the pulses certainly is singular, and the modulations seem to evolve slowly.

Remark 8.1. Even for $\varepsilon \gg \varepsilon_{\text{split}}$ there can still be spatially-periodic multi-pulse patterns. Heuristically, for ε large, but not too large, this follows from the fact that the maximum value of U in a pulse interval increases monotonically (without bound) as the wave length decreases [2, 3]; *i.e.*, the effective value of ε can ‘always’ be reduced below $\varepsilon_{\text{split}}$. Once ε becomes too large, however, then this heuristic ‘scheme’ is no longer applicable, since the V -pulses lose their singular structure and the wave length of the periodic patterns becomes smaller and smaller as ε increases (see Figure 10 in [2] and see [18]). This regime is studied in detail in [18], where it is shown that eventually the periodic solutions no longer ‘touch down’ on the slow manifold (in the phase space), and they become non-singular periodic orbits. Moreover, it is shown there that these orbits are finally annihilated in a Turing/Ginzburg-Landau bifurcation in the PDE (which is manifested in the associated ODE as a reversible 1 : 1 resonant Hopf bifurcation).

Remark 8.2. The above explanation of why traveling pulses will only split after a certain (long) time can be interpreted as a reformulation into more geometrical terms of the arguments given in subsection 3.5: ‘perturbations’ that can be assumed to be small enough immediately after the first splitting will grow slowly as time evolves.

8.2 Strongly coupled pulses

In subsection 8.1, we focused on the significance of the slowly-modulated two-pulse solutions for the self-replication process. As we have shown in Sections 3-7, however, these solutions exist and are stable for all parameter combinations within the region presented in Figure 3, *i.e.*, not just near C_{SPLIT} . In Figure 2a, we have shown a simulation of such an asymptotically stable slowly-modulated two pulse solution, where we refer to subsection 8.3 for a discussion of the effects of a

bounded domain.

The analysis of two-pulse solutions in this paper can be interpreted as a study of *strongly coupled pulses* in singular perturbed reaction-diffusion equations, as mentioned in the Introduction. This coupling is ‘strong,’ since the U -components of the solutions are not assumed to be close to the trivial state $U = 1$ and, in fact, vary by $\mathcal{O}(1)$ amounts. Hence, the interaction between the two modulating pulses is stronger than that which occurs only via exponentially small ‘tail-interactions.’

As was shown in Section 3 for Case **Ia**, the general result is that the separation distance $2\Gamma(t)$ obeys a highly nonlinear ODE (3.31), which is valid for any $\mathcal{O}(1)$ value of Γ . The right hand side of the ODE (3.31) contains both a denominator, which is important for accurately describing the rate of change of Γ for small to medium values of Γ , and a numerator, which captures the long term dynamics to leading order after Γ has become sufficiently large. In particular, in terms of the scaling (5.25), $\Gamma(\tau)$ has become sufficiently large already for $\Gamma(\tau) = \mathcal{O}(\ln \tau)$ with $\tau \gg 1$. In this regime, the ODE (3.31) reduces to

$$\frac{d\Gamma}{d\tau} = \frac{2}{3\sqrt{A}} e^{-2\sqrt{A}\Gamma(\tau)},$$

which is precisely the equation that is appropriate for describing weakly coupled pulses, since $U_{\max}(\tau)$ has approached $U = 1$ (see (5.17)) and $c(t)$ has become $\ll 1$.

Moreover, translating this equation for the weak interaction limit into an equation written in terms of the scaled speed $\hat{c}(\tau)$, one gets to leading order

$$\frac{d\hat{c}}{d\tau} = -2\hat{c}^2.$$

Hence, this equation obtained for the limiting weak interactions is a significantly simplified version than that (3.32), (5.20) derived in Sections 3 and 5 for strong interactions.

Remark 8.3. The form of the equation just obtained for sufficiently large Γ agrees with that of the equation determined concurrently in [8] for pulse interactions in the Gray-Scott model. The results in [8] apply to more general equations which satisfy the requirement that the separation distance between the two pulses exceed some threshold so that the concentrations of all species are exponentially close to their homogeneous steady state values.

Remark 8.4. In order to present a detailed description of the dynamics during splitting events, one needs a method to study ‘fully interacting’ pulses, which is stronger than that used to study ‘strongly interacting’ pulses in this paper (where it is always assumed that the V -pulses of the modulating two pulse solutions are separated). This is because the splitting process itself is a relatively fast one (see for instance [21] and Figure 6 in [2]) and hence the quasisationary approach developed here is no longer applicable. So far, a detailed quantitative description of the behavior of (U, V) for fully interacting pulses does not yet exist. See [24, 25] and [21, 8] for completely different approaches to the details of this splitting process.

Remark 8.5. The methods developed in this paper for modulating two-pulse solutions can be extended to strong pulse interactions in more general singular reaction-diffusion equations, including the (generalized) Gierer-Meinhardt model [5], [20].

8.3 Solutions on bounded domains, four-pulse solutions

In the parameter regime in which the two-pulse solutions have been shown to exist and be stable on unbounded domains, we found that both pulses travel with a speed c that decreases slowly to 0 (as $1/\tau$) and hence that the distance $2\Gamma(\tau)$ between the pulses becomes unbounded. The analysis on bounded domains differs a bit from that carried out in this paper since there are now two homogeneous Neumann boundary conditions that have to be imposed, one at each end of the interval. In geometric terms, this implies that we construct an orbit that ‘jumps’ from a hyperbolic cosine solution (5.14) on \mathcal{M} to another hyperbolic cosine solution on \mathcal{M} . By following the geometric method developed in this paper, therefore, one may obtain ODE’s for the speeds $c_i(\tau)$ in each interval.

Numerically, we observe that a two-pulse solution will slow down faster than the rate given by the ODE (3.32), (5.20) for c , due to the interaction with the boundaries. This comparison was done for a sequence of L values with the largest values corresponding to an ‘infinite’ domain. In these cases, two-pulse solutions converge toward the (asymptotically stable) periodic two-pulse solution [3, 18] so that $\Gamma(\tau) \rightarrow L/4$, where L is the length of the interval. See Appendix A for a short discussion of the effect of having a bounded interval on the methods developed in this paper.

The interactions of the two-pulse solutions with the boundaries of the domain can lead to significantly different, and unexpected, behavior near the splitting bifurcation at $\varepsilon_{\text{split}}$. See Figure 8. This periodic behavior disappears as L is increased.

In this paper, we did not pay attention to the analysis of the 4-pulse solutions that appear after the second splitting (*i.e.* the first splitting of the traveling two-pulse), etc... or to any solutions with more pulses. These solutions can be constructed using the same method as used in the previous sections. For example, for four-pulse patterns, one introduces a function $X_{\text{split}}(\tau)$ and divides the real line into four regions, $(-\infty, -X_{\text{split}}(\tau))$, $(-X_{\text{split}}(\tau), 0)$, $(0, X_{\text{split}}(\tau))$ and $(X_{\text{split}}(\tau), \infty)$. Then, the interior intervals support hyperbolic cosine solutions that satisfy Neumann boundary conditions.

8.4 Cross-fertilization between the analytical and geometrical approaches

The two methods used in this paper for showing existence of modulating two-pulse solutions were developed simultaneously, and each profited from the insights provided by the other. The analytical approach to singular perturbation theory offers clear insights as to how to find the general scalings of the independent and dependent variables. As stated in Sections 2 and 3, only one essential Ansatz is made at the beginning of the analysis, namely that the spatial variations of U and V occur on widely disparate length scales. The length scale for the activator concentration V , which is precisely the pulse width, was found (see (2.2) and (3.6)) directly from the equation for V assuming U to be constant to leading order in the pulse interval. Then, the other scalings, namely the scaling of U (see (2.14) and (3.28)), the wave speed $c(t)$ (see (3.30)), and the global condition (2.15), were delayed as long as possible and were determined during the course of the analysis. By contrast, the method based on geometric singular perturbation theory, while it begins with these scalings (see (4.2)), provides clear insight into the central structures in phase space, as well as into how they vary with parameters. Geometrically, the persistent homoclinic orbits to the slow manifold

correspond to the fast (or inner) pulse solutions. Also, the dynamics of orbits on the slow manifold \mathcal{M} precisely gives the slow evolution of U outside the pulse intervals, *i.e.*, the outer solutions.

Finally, the geometric method leads directly to the identification of all four subcases **Ia-IIb**, with the structural differences being clear from the dynamics on the slow manifold, see Figure 5. In addition, it demonstrates constructively that the solutions constructed by the analytical approach actually exist, and it leads naturally to the various bifurcations, as well as to the understanding of the maximum wave speeds. Of course, the existence results derived from both methods agree. For example, in the analysis of Case **Ia**, which is the only subcase for which we present both methods, the same conditions for the existence (compare (3.19) and (3.25) with the Melnikov criterion (5.6) and (5.7)) and the same ODEs for $c(t)$ (compare (3.32) with (5.20)) are found.

Acknowledgements. A.D. gratefully acknowledges support from the Netherlands Organization for Scientific Research (NWO). W.E. is grateful to his co-authors for introducing him to this problem. T.K. gratefully acknowledges support from the National Science Foundation through CAREER grant DMS-9624471 and from the Alfred P. Sloan Foundation in the form of a Sloan Research Fellowship (1995-1998, when most of this work was carried out). We also thank Paul Zegeling for useful conversations. Finally, we thank A. Harkin and D. Morgan for their help in making the figures.

A The effects of a finite interval for a stationary single-pulse

In [2], the numerical simulations were done on a finite interval, say $x \in [-L, L]$, and it was shown experimentally that, if the interval is large enough, changing the length does not affect the numerical solution.

We shall analyze here the finite-interval problem (with Dirichlet boundary conditions), by the method of Section 2. The main task is to “solve” the equation (2.1) for $u(x)$ with boundary conditions $u = 1$ for $x = \mp L$. This is an elementary exercise, but the formulas are lengthy. So, we introduce the abbreviation

$$f(x') = u(x')v^2(x'). \quad (\text{A.1})$$

Instead of (2.4), one gets

$$u(x) = 1 - \frac{1}{2\sqrt{A}} \left\{ e^{-\sqrt{A}x} \left[C_1 + \int_{-L}^x e^{\sqrt{A}x'} f(x') dx' \right] + e^{\sqrt{A}x} \left[C_2 + \int_x^L e^{-\sqrt{A}x'} f(x') dx' \right] \right\}, \quad (\text{A.2})$$

with

$$C_1 = \frac{1}{2\sinh 2L\sqrt{A}} \left[e^{-2L\sqrt{A}} \int_{-L}^L e^{\sqrt{A}x'} f(x') dx' - \int_{-L}^L e^{-\sqrt{A}x'} f(x') dx' \right], \quad (\text{A.3})$$

$$C_2 = \frac{1}{2\sinh 2L\sqrt{A}} \left[e^{-2L\sqrt{A}} \int_{-L}^L e^{-\sqrt{A}x'} f(x') dx' - \int_{-L}^L e^{\sqrt{A}x'} f(x') dx' \right]. \quad (\text{A.4})$$

These formulas greatly simplify when using the same approximations as in Section 2, that is, by considering the pulse-function $v^2(x)$ to act approximately as a delta function in the integrals. One thus obtains $C_2 = C_1$ where:

$$C_1 = \frac{ku_0}{2\sinh 2L\sqrt{A}} \left[e^{-2L\sqrt{A}} - 1 \right]. \quad (\text{A.5})$$

Furthermore

$$u(x) \cong 1 - \frac{1}{2\sqrt{A}} \left\{ e^{-\sqrt{A}x} \left[C_1 + \int_{-L}^x v^2(x') dx' \right] + e^{\sqrt{A}x} \left[C_2 + \int_x^L v^2(x') dx' \right] \right\}. \quad (\text{A.6})$$

The crucial quantity in further analysis is u_0 . From (A.6), we get

$$u_0 = 1 - \frac{ku_0}{2\sqrt{\varepsilon}} \left[1 + \frac{e^{-2L\sqrt{A}} - 1}{\sinh 2L\sqrt{A}} \right]. \quad (\text{A.7})$$

It is, therefore, clear that when L is large enough the correction due to the finite interval is exponentially small. As in [24, 2, 25, 3] we performed numerical simulations of (1.1) in this paper with the typical values $A = \mathcal{O}(D) \ll 1$ and $2L = 100$, so that $2L\sqrt{A} = \mathcal{O}(1/\sqrt{D}) \gg 1$, and the effect of finite interval is indeed negligible.

B Stability analysis in Case IIa

The substitution of $\delta = \sigma\varepsilon$ into the full eigenvalue problem (7.7) yields:

$$\begin{aligned} u_{\xi\xi} &= \varepsilon^2 \left(v_0^2 u + 2u_0 v_0 v \right) + \varepsilon^4 \sigma^2 u + D\lambda u - D\varepsilon^2 c u_\xi \\ v_{\xi\xi} + (2u_0 v_0 - (1 + \lambda))v &= -v_0^2 u - \varepsilon^2 c v_\xi, \end{aligned} \quad (\text{B.1})$$

with $u_0 = u_-$. We restrict our attention in this Appendix to the regime in which $D \ll \varepsilon^4 \sigma^2$. i.e. the regime left of $\mathcal{C}_{\text{Hopf}}$ in Figure 3.

Since the leading order slow eigenvalue problem is $u_{\xi\xi} = \varepsilon^4 \sigma^2 u$ (recall v_0 is exponentially small), the jump discontinuity in u_ξ at $\xi = 0$ ($x = 0$) in the slow field is to leading order:

$$\Delta_s u_\xi = -2\varepsilon^2 \kappa \sigma. \quad (\text{B.2})$$

The same jump discontinuity measured in the fast field is:

$$\Delta_f u_\xi = \varepsilon^2 \left(\frac{6\kappa}{u_0^2} + 2u_0 \int_{-\infty}^{\infty} v_0(\xi)v(\xi)d\xi \right). \quad (\text{B.3})$$

Hence, the matching condition, *i.e.*, equating (B.2) and (B.3), yields:

$$\kappa = \frac{-u_0^3}{3 + \sigma u_0^2} \int_{-\infty}^{\infty} v_0(\xi)v(\xi)d\xi, \quad (\text{B.4})$$

where κ is the constant, leading order value of u inserted into the NLEP (7.16).

As in subsection 7.2.1 here and in Section 5 of [3], we may further transform this NLEP by setting $t = \xi/2$, $y(t) = v(\xi)$, and again using $P^2 = 4(1 + \lambda)$ and $v_0 = (3/2u_0)\text{sech}^2(\xi/2)$:

$$\ddot{y} + \left(12\text{sech}^2(t) - P^2 \right) y = \frac{27}{3 + \sigma u_0^2} \text{sech}^4(t) \int_{-\infty}^{\infty} y(t)\text{sech}^2(t)dt. \quad (\text{B.5})$$

Now, we introduce a new parameter m via the implicit formula:

$$\frac{1 - \sqrt{1 - 6c - 12\sigma}}{c + 2\sigma} = m \left(\frac{1 - \sqrt{1 - 12\sigma}}{2\sigma} \right). \quad (\text{B.6})$$

The parameter m indexes the slowly-modulated two pulse solutions (in a 1-1 fashion with c), and:

$$m \in \left(1, \frac{12\sigma}{1 - \sqrt{1 - 12\sigma}} \right), \quad (\text{B.7})$$

so that m must be 1 in the limit as $\sigma \rightarrow 1/12$ (and $c \rightarrow 0$) and $m \in (1, 2)$ in the limit as $\sigma \rightarrow 0$. Therefore, we may write the constant coefficient on the right of the NLEP (B.5) as:

$$C = \frac{27}{3 + \sigma u_-^2} = \frac{54\sigma}{6\sigma + m^2 [1 - 6\sigma - \sqrt{1 - 12\sigma}]}. \quad (\text{B.8})$$

The compatibility condition also used in subsection 7.3, namely formula (5.12) from [3], gives C as a function of P (see also subsection 7.2). In particular, we set $C = \mathcal{C}(P)$ in (B.8) and thereby

obtain the graph of a function σ of P which will be used to determine the location of the eigenvalues λ with positive real parts, if any, for positive values of the parameter σ . A little algebra with (B.8) shows that $m^2\mathcal{C}\sqrt{1-12\sigma} = m^2\mathcal{C} + 6\sigma(\mathcal{C} - m^2\mathcal{C} - 9)$, and hence it has solutions only if

$$m^2\mathcal{C} + 6\sigma(\mathcal{C} - m^2\mathcal{C} - 9) \geq 0,$$

because the fact that the left hand side is nonnegative implies that the right hand side must be, as well. Stated in terms of σ , this requirement is:

$$\sigma \leq \sigma_1(P) = \frac{m^2\mathcal{C}}{6(9 + (m^2 - 1)\mathcal{C})}, \quad (\text{B.9})$$

and one may observe that σ_1 is a monotonically decreasing function of P , with $\sigma_1(P = 2) = m^2/(6(m^2 + 1))$ since $\mathcal{C}(P = 2) = 9/2$ and $\sigma_1(P = 3) = 0$ since $\mathcal{C}(P = 3) = 0$ [3]. Now, simplifying the above identity involving $(\mathcal{C} - m^2\mathcal{C} - 9)$, we get:

$$-m^4\mathcal{C}^2\sigma = m^2\mathcal{C}\sigma[\mathcal{C} - m^2\mathcal{C} - 9] + 3\sigma^2[\mathcal{C} - m^2\mathcal{C} - 9]^2.$$

Hence, the solution is either $\sigma = 0$, as found in the $\sigma \ll 1$ case of subsection 7.2, or:

$$\sigma_\kappa(P) = \frac{m^2\mathcal{C}(9 - \mathcal{C})}{3(9 - (1 - m^2)\mathcal{C})^2}. \quad (\text{B.10})$$

The function $\sigma_\kappa(P)$ is a monotone function of $\mathcal{C} = \mathcal{C}(P)$. At the two endpoints of the P -interval under consideration it simplifies to

$$\sigma_\kappa(P = 2) = \frac{m^2}{3(1 + m^2)^2} \quad \text{since } \mathcal{C}(P = 2) = \frac{9}{2}, \quad \text{and} \quad \sigma_\kappa(P = 3) = 0 \quad \text{since } \mathcal{C}(P = 3) = 0.$$

In between these endpoints, $\sigma_\kappa(P)$ is a monotonically decreasing function of P .

Thus, the function $\sigma_\kappa(P)$ lies below $\sigma_1(P)$ at $P = 2$. In addition, at $P = 3$, where both functions vanish, one readily calculates that σ_κ has the more negative slope. Hence, the two curves $\sigma_1(P)$ and $\sigma_\kappa(P)$ must intersect at some point $(P_*, \sigma_*(m))$ where $P_* \in (2, 3)$ and $0 < \sigma_*(m) < m^2/(3(1+m^2)^2)$. Therefore, for any m under consideration, the slowly modulated two pulse solution is formally stable with respect to small perturbations when $\sigma < \sigma_*(m)$. In the special case of $m = 1$, we have $\sigma_*(m = 1) = 1/12$, and hence we recover that the stationary homoclinic is stable in this regime.

References

- [1] J.G. Blom, P.A. Zegeling [1994], Algorithm 731: A Moving-Grid Interface for Systems of One-Dimensional Time-Dependent Partial Differential Equations, *ACM Transactions in Mathematical Software*, **20**, 194–214.
- [2] A. Doelman, T.J. Kaper, and P. Zegeling [1997], Pattern formation in the one-dimensional Gray-Scott model, *Nonlinearity*, **10**, 523–563.
- [3] A. Doelman, R. A. Gardner and T.J. Kaper [1998], Stability analysis of singular patterns in the 1-D Gray-Scott model: a matched asymptotics approach, *Physica D*, **122**, 1–36.

- [4] A. Doelman, R. A. Gardner and T.J. Kaper [1998], A stability index analysis of 1-D patterns of the Gray–Scott model, submitted.
- [5] A. Doelman, R. A. Gardner and T.J. Kaper [1999], Large stable pulse solutions in reaction-diffusion equations, in preparation.
- [6] W. Eckhaus [1979], ‘*Asymptotic Analysis of Singular Perturbations*’, North-Holland Publishing Company, Amsterdam.
- [7] W. Eckhaus and R. Kuske [1997], Pattern formation in systems with slowly varying geometry, *SIAM J. Appl. Math.* **57**, 112–152.
- [8] S. Ei, Y. Nishiura, and B. Sandstede [1999], Pulse-interaction approach to self-replicating dynamics in reaction-diffusion systems (in preparation).
- [9] C. Elphick, A. Hagberg and E. Meron [1995], Dynamical front transitions and spiral vortex nucleation, *Phys. Rev. E*, **51**, 3052-3058.
- [10] N. Fenichel [1979], Geometrical singular perturbation theory for ordinary differential equations, *J. Diff. Eq.*, **31**, 53–98.
- [11] P. Gray and S.K. Scott [1984], Autocatalytic reactions in the isothermal, continuous stirred tank reactor: oscillations and instabilities in the system $A + 2B \rightarrow 3B$, $B \rightarrow C$, *Chem. Eng. Sci.*, **39**, 1087–1097.
- [12] J.K. Hale, L.A. Peletier, and W.C. Troy [1998], Exact homoclinic and heteroclinic solutions of the Gray-Scott model for autocatalysis, to appear in *SIAM J. Appl. Math.*, University of Leiden, Mathematics Department, Technical Report Number W98-03.
- [13] J.K. Hale, L.A. Peletier, and W.C. Troy [1999], Stability and instability in the Gray-Scott model: the case of equal diffusivities, *Appl. Math. Lett.* **12**, 59–65.
- [14] C.K.R.T. Jones [1995], Geometric singular perturbation theory, in *Dynamical systems, Montecatini Terme, 1994*, Lecture Notes in Mathematics, **1609**, R. Johnson (ed.), Springer-Verlag.
- [15] B.S. Kerner and V.V. Osipov [1994], *Autosolitons: a new approach to problems of self-organization and turbulence*, Kluwer, Dordrecht.
- [16] K.J. Lee and H.L. Swinney [1995], Lamellar structures and self-replicating spots in a reaction-diffusion system, *Phys. Rev. E*, **51**, 1899-1915.
- [17] K.-J. Lin, W.D. McCormick, J.E. Pearson, and H.L. Swinney [1994], Experimental observation of self-replicating spots in a reaction-diffusion system, *Nature*, **369**, issue no. 6477, 215–218.
- [18] D.S. Morgan, A. Doelman and T.J. Kaper [1998], Stationary periodic orbits in the 1-D Gray-Scott model, Technical Report **13**, Center for BioDynamics, Boston Univ., *submitted*.
- [19] C. Muratov and V. Osipov, [1998] Spike autosolitons in the Gray-Scott model, preprint.
- [20] W.-M. Ni [1998], Diffusion, cross-diffusion, and their spike-layer steady states, *Notices AMS*, **45**(1), 9–18.
- [21] Y. Nishiura and D. Ueyama [1999], A skeleton structure for self-replication dynamics, to appear in *Physica D*.

- [22] J.E. Pearson [1993], Complex patterns in a simple system, *Science*, **261**, 189–192.
- [23] V. Petrov, S.K. Scott, and K. Showalter [1994], Excitability, wave reflection, and wave splitting in a cubic autocatalysis reaction-diffusion system, *Phil. Trans. Roy. Soc. Lond., Series A*, **347**, 631–642.
- [24] W.N. Reynolds, J.E. Pearson, and S. Ponce-Dawson [1994], Dynamics of self-replicating patterns in reaction diffusion systems, *Phys. Rev. Lett.*, **72**, 2797–2800.
- [25] W.N. Reynolds, S. Ponce-Dawson, and J.E. Pearson [1997], Self-replicating spots in reaction-diffusion systems, *Phys. Rev. E*, **56**, 185–198.
- [26] C. Robinson [1983], Sustained resonance for a nonlinear system with slowly-varying coefficients, *SIAM J. Math. Anal.*, **14**, 847–860.
- [27] A. van Harten [1978], Nonlinear singular perturbation problems: proofs of correctness of a formal approximation based on a contraction principle in a Banach space, *J. Math. Anal. Appl.* **65**, 126–168.

Figure captions

Figure 1. (a) A two-pulse solution shown at time $t = 500$ that is obtained from numerical simulations of the PDE (1.1) with parameter values $A = 0.01$, $B = 0.0696$ and $D = 0.01$. The U component is shown dashed, with U reaching a local maximum in between the V pulses (solid curve) at $U_{\max} \approx 0.194$. The two pulses move apart from each other with slowly varying speeds $c(t)$, and the U component is an $\mathcal{O}(1)$ distance away from the homogeneous state in between the pulses, even though the pulses are quite far apart and the V component (solid curve) is exponentially small there. (b) The solution (U, V) from the same initial data shown at a later time ($t = 5,000$), and the value of U_{\max} has slowly risen to ≈ 0.730 .

Figure 2. (a) Time evolution of the V component of a modulating two-pulse solution of (1.1) with $A = 0.01$, $B = 0.0696$ and $D = 0.01$, *i.e.*, below $\varepsilon_{\text{split}}$. (b) A numerical simulation of pulse splitting in (1.1), showing V pulses with slowly decreasing speeds which split when the speeds are small. The parameter values are $A = 0.01$, $B = 0.0674$ and $D = 0.01$. In both plots, the vertical axis is $1,400V + t$ (where by default we use $T_{\text{end}}/10$ as the multiple of V), and $L = 100$.

Figure 3. A summary of the existence and stability results obtained in this paper, shown in the limit $0 < D \ll 1$. The scalings $A = D^\alpha$ and $B = D^\beta$ are used for this figure only. The lines shown are \mathcal{C}_{SN} : $\beta = (\alpha/3) - (1/3)$ (see subsection 6.2); $\mathcal{C}_{\text{SPLIT}}$: $\beta = \alpha/2$ (see the Introduction and subsection 8.1); \mathcal{C}_{TW} : $\beta = (\alpha/3) + (1/3)$ (see subsection 6.1); and, $\mathcal{C}_{\text{HOPF}}$: $\beta = (\alpha/2) - (1/4)$ (identified in Remark 7.3).

Figure 4. A stationary one-pulse solution of (1.1) whose existence is demonstrated in Section 2 and in [2]. The parameter values are $A = 0.01$, $B = 0.1423$, and $D = 0.01$.

Figure 5. A schematic illustration of the geometries on the slow manifolds in each of the four distinct subcases identified in this paper. Frames (a)-(d) correspond to subcases **Ia-IIb**, respectively. In (a) and (b), the dashed segment on the u -axis indicates that $\varepsilon/\delta \gg 1$. In (a) and (c), the restricted manifolds ℓ^U and ℓ^S are symmetric about the u -axis, whereas they are not symmetric in frames (b) and (d).

Figure 6. A schematic illustration of the rightward moving slowly-modulating pulse in the phase space of the ODE (4.6) at a fixed instant of time t . The thickest curve corresponds to the singular orbit for the slowly-modulating pulse, with the horizontal segment being a projection of the homoclinic excursion in the fast field onto the slow manifold \mathcal{M} . The curves T_o and T_d , as well as the restricted stable and unstable manifolds ℓ^S and ℓ^U , are also shown.

Figure 7. Time evolution of the V component of a modulating two-pulse solution of (1.1) with $A = 0.01$, $B = 0.0474$ and $D = 0.01$, so that ε lies even further from $\varepsilon_{\text{split}}$. The outermost pulses appear to propagate at constant speed while significant oscillations take place on the trailing edges before the splitting. The vertical axis is $700V + t$.

Figure 8. A numerical simulation of (1.1) on a domain of length $L = 100$ with parameters $A = 0.01$, $B = 0.0676$, and $D = 0.01$ which exhibits significant periodic oscillations (at least up to time 30,000) that are due to boundary effects. The parameter values are extremely close to $\varepsilon_{\text{split}}$. The vertical axis is $3000V + t$. This figure illustrates the fact that sufficiently large domains must be used before determining if particular parameter values give rise to asymptotically stable two-pulse solutions or to splitting.

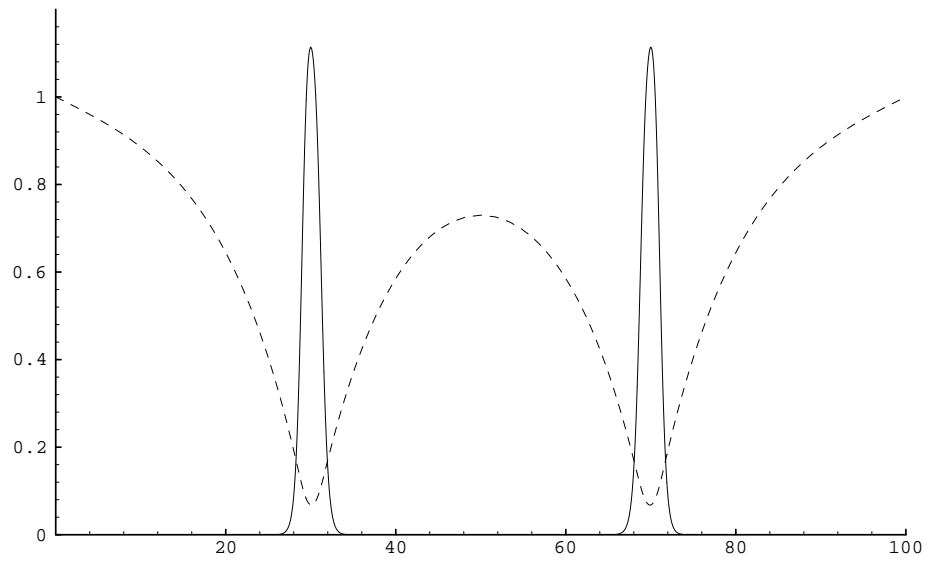
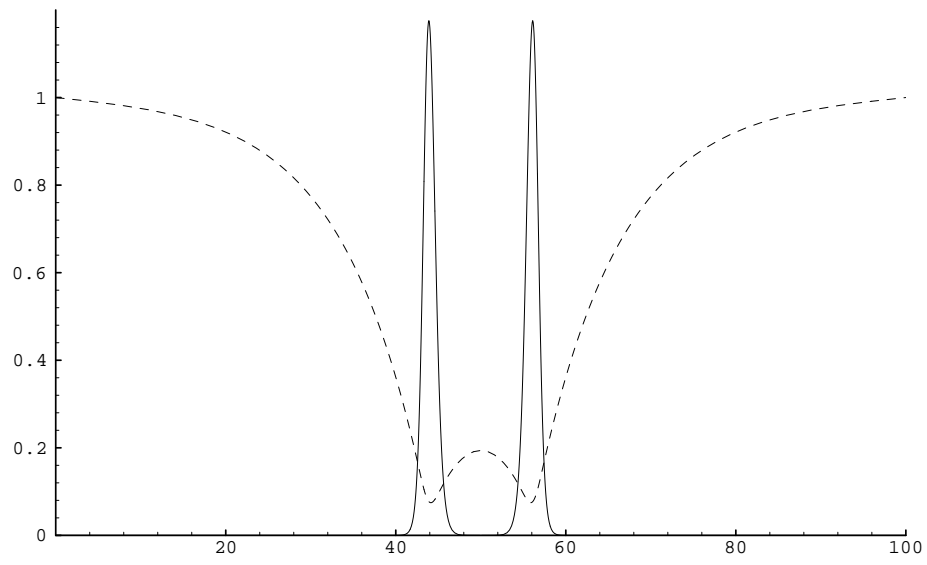


Figure 1:

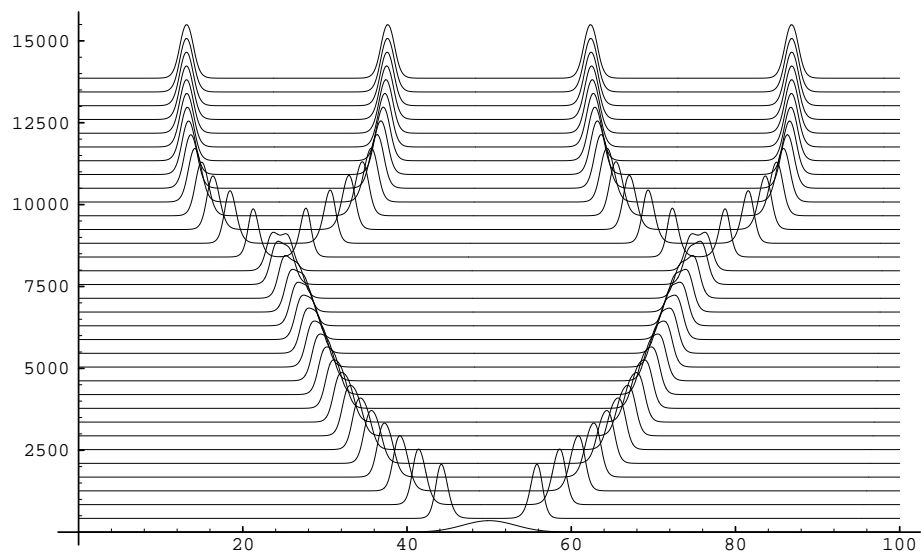
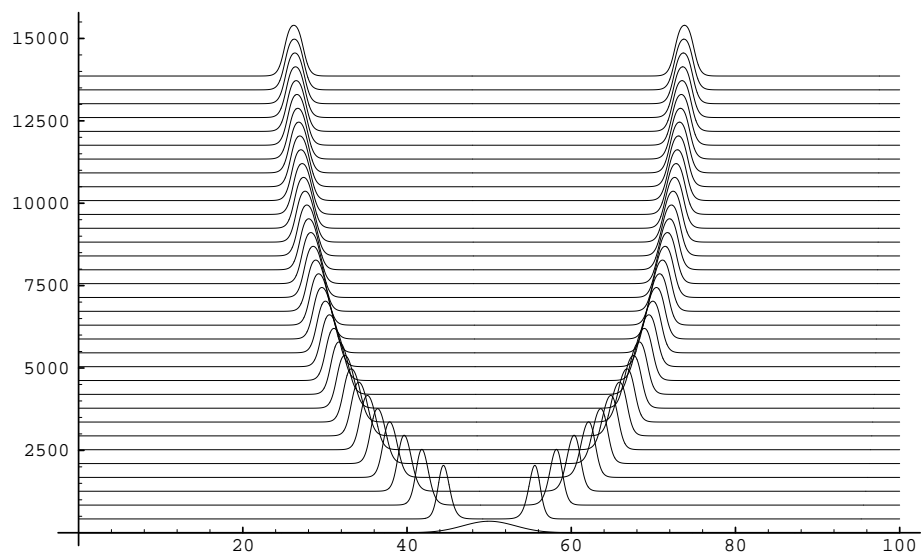


Figure 2:

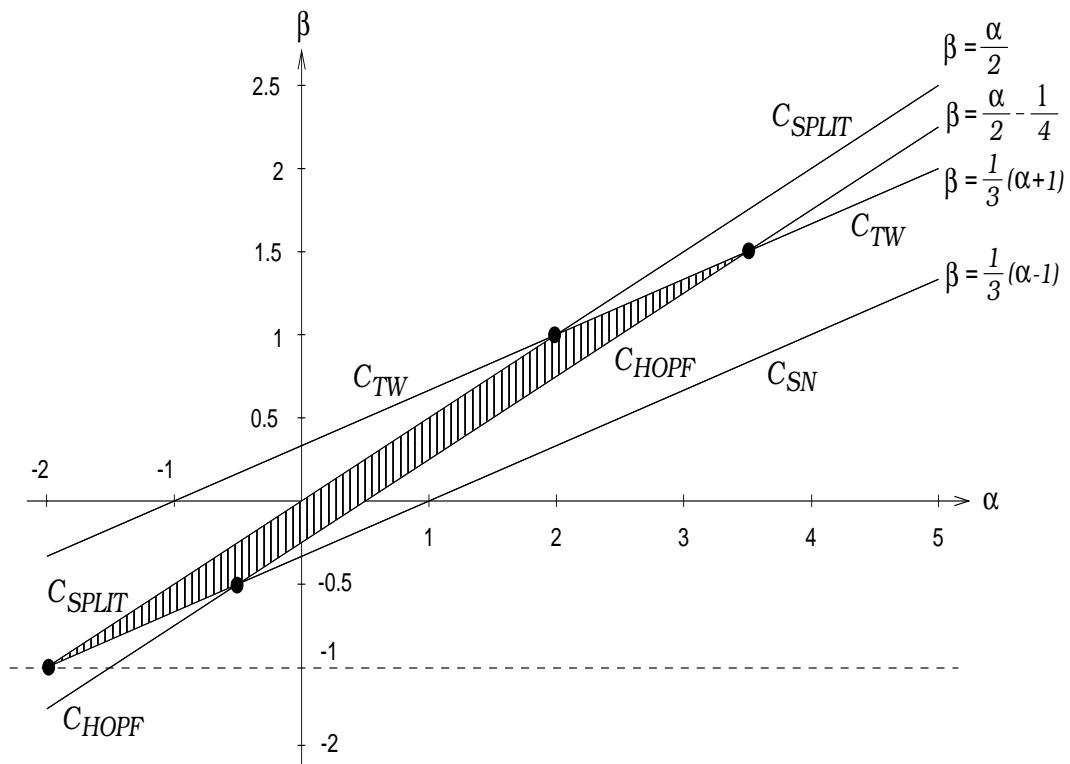


Figure 3:

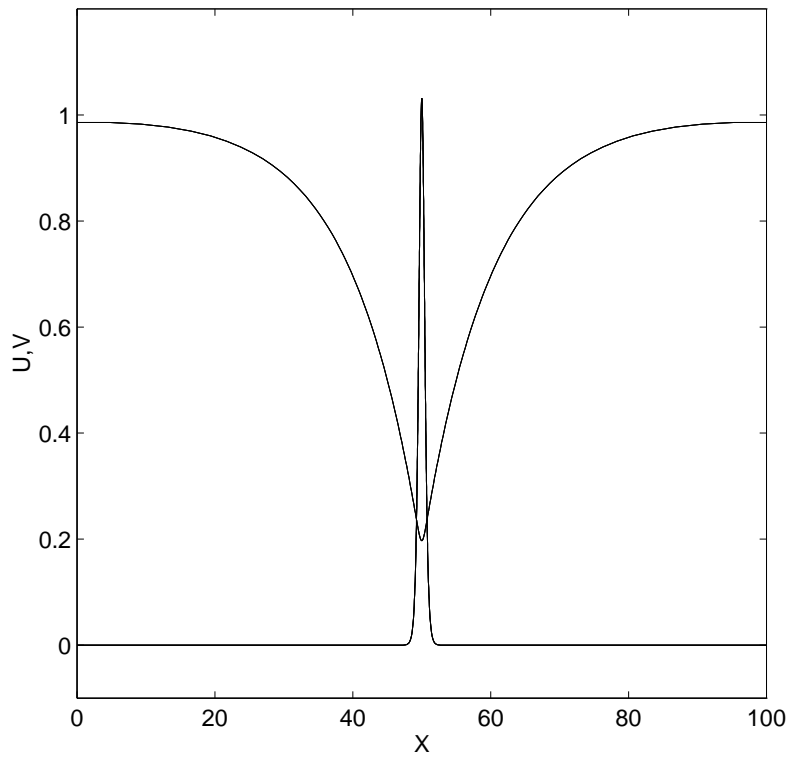


Figure 4:

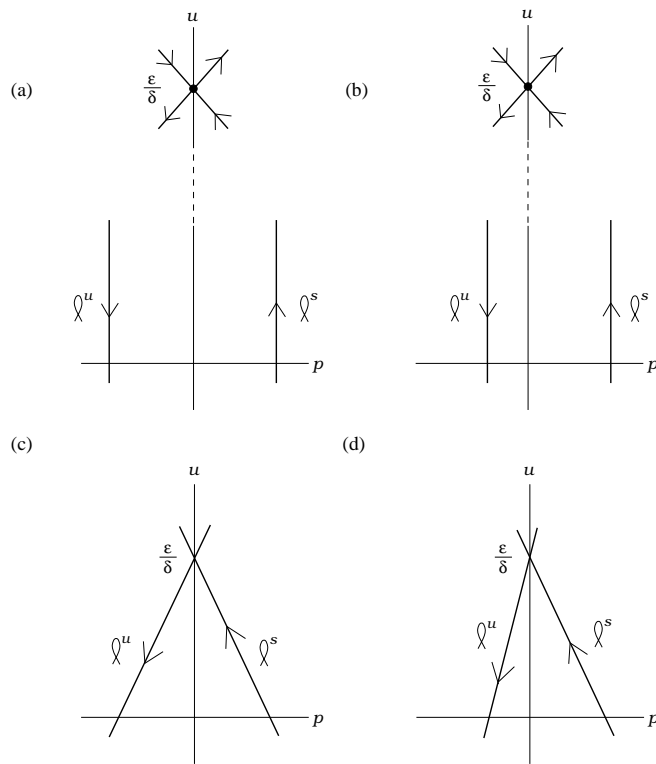


Figure 5:

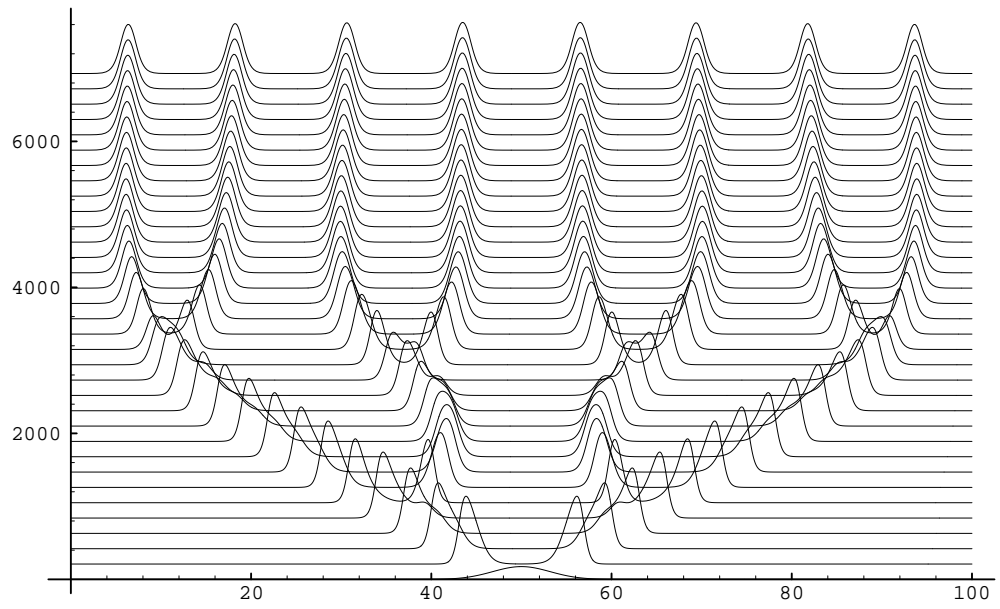


Figure 7:

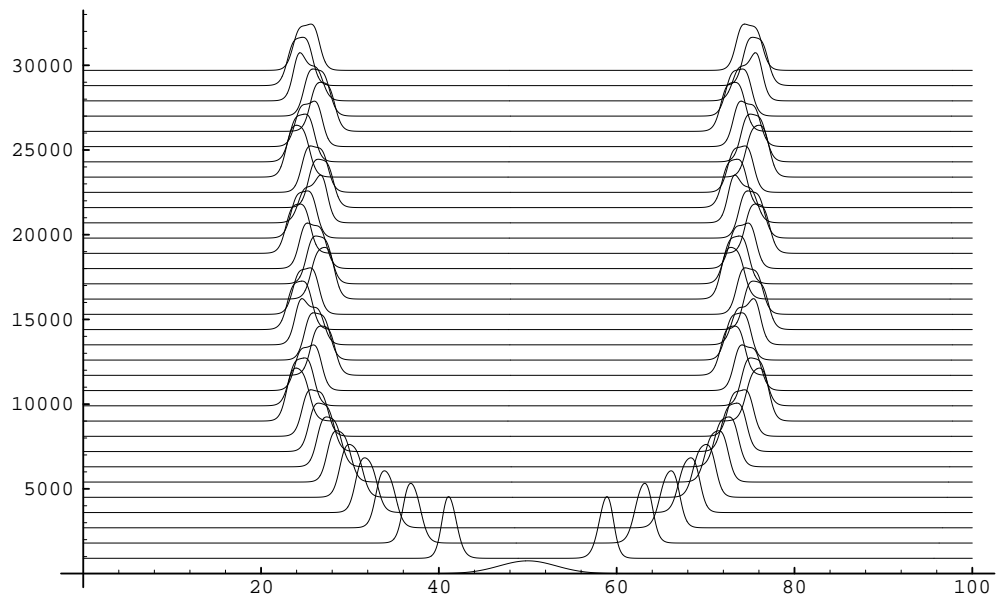


Figure 8: